

# **Inorganic Polymer Derived Ceramic Membranes 2**

**1006557**

Final Report, November 2001

EPRI Project Manager  
W. Bakker

## **DISCLAIMER OF WARRANTIES AND LIMITATION OF LIABILITIES**

THIS DOCUMENT WAS PREPARED BY THE ORGANIZATION(S) NAMED BELOW AS AN ACCOUNT OF WORK SPONSORED OR COSPONSORED BY THE ELECTRIC POWER RESEARCH INSTITUTE, INC. (EPRI). NEITHER EPRI, ANY MEMBER OF EPRI, ANY COSPONSOR, THE ORGANIZATION(S) BELOW, NOR ANY PERSON ACTING ON BEHALF OF ANY OF THEM:

(A) MAKES ANY WARRANTY OR REPRESENTATION WHATSOEVER, EXPRESS OR IMPLIED, (I) WITH RESPECT TO THE USE OF ANY INFORMATION, APPARATUS, METHOD, PROCESS, OR SIMILAR ITEM DISCLOSED IN THIS DOCUMENT, INCLUDING MERCHANTABILITY AND FITNESS FOR A PARTICULAR PURPOSE, OR (II) THAT SUCH USE DOES NOT INFRINGE ON OR INTERFERE WITH PRIVATELY OWNED RIGHTS, INCLUDING ANY PARTY'S INTELLECTUAL PROPERTY, OR (III) THAT THIS DOCUMENT IS SUITABLE TO ANY PARTICULAR USER'S CIRCUMSTANCE; OR

(B) ASSUMES RESPONSIBILITY FOR ANY DAMAGES OR OTHER LIABILITY WHATSOEVER (INCLUDING ANY CONSEQUENTIAL DAMAGES, EVEN IF EPRI OR ANY EPRI REPRESENTATIVE HAS BEEN ADVISED OF THE POSSIBILITY OF SUCH DAMAGES) RESULTING FROM YOUR SELECTION OR USE OF THIS DOCUMENT OR ANY INFORMATION, APPARATUS, METHOD, PROCESS, OR SIMILAR ITEM DISCLOSED IN THIS DOCUMENT.

ORGANIZATION(S) THAT PREPARED THIS DOCUMENT

**The University of New Mexico**

## **ORDERING INFORMATION**

Requests for copies of this report should be directed to EPRI Customer Fulfillment, 1355 Willow Way, Suite 278, Concord, CA 94520, (800) 313-3774, press 2.

Electric Power Research Institute and EPRI are registered service marks of the Electric Power Research Institute, Inc. EPRI. ELECTRIFY THE WORLD is a service mark of the Electric Power Research Institute, Inc.

Copyright © 2001 Electric Power Research Institute, Inc. All rights reserved.

# CITATIONS

---

This report was prepared by

The University of New Mexico  
Center for Micro-Engineered Materials  
Albuquerque, NM 87131

Principal Investigators

C. J. Brinker

C. M. Braunbarth

G. Xomeritakis

This report describes research sponsored by EPRI.

The report is a corporate document that should be cited in the literature in the following manner:

*Inorganic Polymer Derived Ceramic Membranes 2*, EPRI, Palo Alto, CA: 2001. 1006557.



# REPORT SUMMARY

---

Ceramic porous membranes capable of molecular sieving represent a promising alternative to energy-intensive distillation or cryogenic separation technologies used for processes such as purification of natural gas, air separation, and flue gas cleanup. Such membranes, fabricated at laboratory scale as part of this study, are capable of operating at temperatures as high as 200°C and can withstand harsh chemical environments and aggressive cleaning after fouling. Their selectivity factors and permeabilities are generally an order of magnitude higher than those of commercially available organic membranes.

## Background

Inorganic membranes would be ideal for pressure-based gas separation applications in the chemical and petrochemical industries. To achieve high selectivity factors and permeability, very thin supported membranes are needed, with very high porosities and a tightly controlled narrow pore size distribution below 0.5 nm. Currently available inorganic membranes generally have pore sizes in the 5-nm range and, thus, offer poor selectivity. Organic membranes have the required pore size but are fragile and have severe temperature limitations. Silica-based sol-gel processing can produce very thin polymeric membranes, which upon drying can develop the required fine pore size distribution and can withstand high temperatures. In phase 1 of this project, single-layer inorganic membranes were produced. This report discusses development of dual-layer membranes, which have both higher permeability and selectivity.

## Objective

To develop microporous inorganic membranes capable of molecular sieving gas separation applications.

## Approach

Using sol-gel processing, polymer physics, fractal geometry, drying theory, and film formation principles, researchers explored several strategies to produce thin inorganic membranes with pore radii varying between 0.2 and 2 nm. The following major processing steps were involved: (1) aggregation of fractal polymers from silica-based sols, (2) deposition of novel alumina silicates, (3) variation of capillary pressure, (4) postdeposition aging of films, (5) partial sintering of films, and (6) pyrolysis of fugitive organic template molecules. Using one or more of the above techniques, researchers deposited membranes on commercially available alumina substrates by dip coating, sol casting, or reactive sol casting. They characterized film porosity by ellipsometry and a surface acoustic wave technique. Finally, they used both single- and mixed-gas transport through supported membranes to determine gas selectivity and permeability.

## **Results**

Several inorganic silicate-based membranes developed in this study proved capable of molecular sieving. Similar to commercial organic membranes, a tradeoff had to be made between selectivity (the gas separation factor) and permeability. For each level of permeability, selectivity of the inorganic membrane was at least one order of magnitude greater than that of organic membranes when using CO<sub>2</sub>/CH<sub>4</sub> as the model gas mixture. The best membranes developed had a dual-layer structure: a mesoporous layer to bridge large pores in the macroporous ceramic substrate and a nanoporous layer to achieve molecular sieving. Using this approach, high selectivity as well as high permeability could be obtained. When using class 10 clean room technology, manufacture of the membranes was found to be very reproducible. Long-term testing indicated that the membranes were stable in hot humid environments for at least 2.5 months. One patent covering this technology has been granted and one is pending.

## **EPRI Perspective**

Development of rugged inorganic gas separation membranes will offer considerable benefits both directly and indirectly for the electric power industry. Lower-cost air separation would benefit advanced coal power plants such as coal gasification combined-cycle plants. Moreover, separation of NO<sub>x</sub> from the flue gas of conventional power plants may provide a low-cost method to decrease NO<sub>x</sub> emissions to a much lower level than presently possible. Indirectly, replacement of energy-intensive distillation and cryogenic processes would probably favor electricity usage somewhat through increased use of circulation pumps in the gas separation process. The dual-layer membranes described in this report are far superior to single-layer membranes discussed in the previous report, TR-106735. Therefore, we feel that the dual-layer membranes are ready for commercial scale-up and could find large-scale applications in natural gas purification, CO<sub>2</sub> sequestration, and removal of NO<sub>x</sub> and other impurities from flue gas.

## **Keywords**

Membranes

Molecular sieves

Gas separation

Silicate polymers

Colloids

## ABSTRACT

---

Ceramic porous membranes capable of molecular sieving represent a promising alternative to energy-intensive distillation or cryogenic separation technologies used for processes such as purification of natural gas, air separation, and flue gas cleanup. In phase 1 of this project, single-layer inorganic membranes were produced. This report discusses development of dual-layer membranes, which have both higher permeability and selectivity. To develop microporous inorganic membranes capable of molecular sieving gas separation applications, researchers explored several strategies to produce membranes with pore radii varying between 0.2 and 2 nm. They deposited membranes on commercially available alumina substrates by dip coating, sol casting, or reactive sol casting. They characterized film porosity by ellipsometry and a surface acoustic wave technique. Finally, they used both single- and mixed-gas transport through supported membranes to determine gas selectivity and permeability. The best membranes developed had a dual-layer structure: a mesoporous layer to bridge large pores in the macroporous ceramic substrate and a nanoporous layer to achieve molecular sieving. Using this approach, high selectivity as well as high permeability could be obtained. When using class 10 clean room technology, manufacture of the membranes was found to be very reproducible. Long-term testing indicated that the membranes were stable in hot humid environments for at least 2.5 months. EPRI believes the dual-layer membranes are ready for commercial scale-up and could find large-scale applications in natural gas purification, CO<sub>2</sub> sequestration, and removal of NO<sub>x</sub> and other impurities from flue gas.



# CONTENTS

---

<b>1 INTRODUCTION .....</b>	<b>1-1</b>
1.1 Inorganic Membranes.....	1-1
1.2 Sol-Gel Processing .....	1-3
1.2.1 Sol-gel chemistry .....	1-3
1.2.2 Drying and Shrinkage .....	1-4
1.3 Pore size control .....	1-5
1.3.1 Solvent and Molecular Templating .....	1-5
1.3.2 Surfactant Templating .....	1-8
1.4 Objectives .....	1-10
<b>2 EXPERIMENTAL.....</b>	<b>2-1</b>
2.1 Sol Preparation .....	2-1
2.2 Membrane deposition.....	2-2
2.3 X-ray Diffraction .....	2-3
2.4 Electron Microscopy (SEM and TEM) .....	2-3
2.5 Thermogravimetry (TGA/DTA) .....	2-3
2.6 Surface Acoustic Wave (SAW) Measurements.....	2-3
2.7 Ellipsometry.....	2-4
2.8 Water Contact Angle Measurements .....	2-4
2.9 Gas Permeation Measurements.....	2-4
<b>3 DUAL-LAYER MEMBRANES.....</b>	<b>3-1</b>
3.1 Approach of Dual-Layer Membranes .....	3-1
3.2 Surfactant-Templated Silica .....	3-2
3.3 Dual-Layer Membranes.....	3-6
3.4. Comparison of Membranes With and Without Sub-layer .....	3-8
3.5 Effect of Feed Flow Rate, Temperature and Pressure Gradient.....	3-13
3.6 Hydrogen Purification and NO <sub>x</sub> Removal .....	3-17

---

<b>4 REPRODUCIBILITY AND LONG-TERM STABILITY .....</b>	<b>4-1</b>
4.1 Effect of Environment During Membrane Formation .....	4-1
4.2 Effect of Calcination Conditions .....	4-5
4.3 Long-term Stability .....	4-7
4.4 Overview of Membrane Formation .....	4-9
<b>5 USE OF LARGER PORE SIZE SUPPORTS .....</b>	<b>5-1</b>
5.1 Deposition by Dip-coating .....	5-1
5.2 Deposition by Aerosol Process .....	5-3
<b>6 COMPARISON TO LITERATURE .....</b>	<b>6-1</b>
<b>7 CONCLUSIONS .....</b>	<b>7-1</b>
<b>8 REFERENCES .....</b>	<b>8-1</b>
<b>9 PUBLICATIONS AND PATENTS .....</b>	<b>9-1</b>

# LIST OF FIGURES

---

Figure 1-1 Steady state film deposition profile during dip coating of silica sol on a porous support. ....	1-4
Figure 1-2 Effect of solvent templating on the pore size of sol-gel based silica membranes. ROH/A2 refers to a film prepared from A2** silica sol and solvent substituted by ROH prior dip coating. ROH accessibility refers to the distribution of pore sizes accessible to ROH. ....	1-6
Figure 1-3 Pore size control by a) solvent templating and b) molecular templating.....	1-7
Figure 1-4 Ternary phase diagram of surfactants in water or oil. ....	1-8
Figure 1-5 Schematic of the liquid crystal templating for formation of mesoporous silica.....	1-9
Figure 1-6 Steady state film deposition profile during dip coating surfactant templated silica sol on a porous support.....	1-10
Figure 2-1 Schematic diagram of the experimental setup for gas permeation measurements. ....	2-6
Figure 3-1 Transmission electron micrographs of C <sub>6</sub> and CTAB templated silica gels. ....	3-3
Figure 3-2 Thermogravimetric analysis (TGA/DTA) of C <sub>6</sub> templated silica xerogel in air at a heating rate of 2 °C/min. The dashed lines indicate the calcination temperatures used to prepare materials for nitrogen adsorption and gas permeation measurements. ....	3-4
Figure 3-3 Nitrogen adsorption isotherm (77K) of both thin silica films (C6 and CTAB templated) and bulk silica xerogel (A2**) after removal of templates by calcination at 500 °C in air.....	3-6
Figure 3-4 Cross-sectional electron micrographs of an asymmetric membrane: (a) SEM overview- (i) SiO <sub>2</sub> membrane (see (b) in details) on top of γ-Al <sub>2</sub> O <sub>3</sub> layer, (ii) asymmetric α-Al <sub>2</sub> O <sub>3</sub> support, and (b) TEM micrograph revealing the dual-layer silica membrane- (iii) A2** top layer, (iv) C6STS sub-layer.....	3-7
Figure 3-5 SEM top-view of a dual layer membrane with C <sub>6</sub> -templated silica sublayer. ....	3-7
Figure 3-6 Comparison of gas permeances of the microporous membrane (A2**) with and without a C <sub>6</sub> -templated sub-layer. (solid symbols correspond to dual layer membranes, open symbols correspond to single layer membrane without sub-layer). ....	3-9
Figure 3-7 Comparison of selectivity of the microporous membrane (A2**) with and without a C <sub>6</sub> -templated sub-layer. (solid symbols correspond to dual layer membranes, open symbols correspond to single layer membrane without sub-layer). ....	3-9
Figure 3-8 Comparison of gas permeances of a BTE/TEOS membrane with and without a mesoporous CTAB-templated sub-layer. (solid symbols correspond to dual layer	

membranes, open symbols correspond to single layer membrane without sub-layer).....	3-11
Figure 3-9 Comparison of selectivity of a BTE/TEOS membrane with and without a mesoporous CTAB-templated sub-layer. (solid symbols correspond to dual layer membranes, open symbols correspond to single layer membrane without sub-layer).....	3-11
Figure 3-10 TEM cross-sectional electron micrograph of a dual-layer micro-porous silica membrane on top of a silicon wafer, (a) silicon wafer, (b) ordered cubic mesoporous silica film templated by Brij-56 block-copolymer surfactant and (c) microporous layer (A2**)......	3-12
Figure 3-11 %CO <sub>2</sub> in permeate and CO <sub>2</sub> /CH <sub>4</sub> separation factor versus stage cut for separation of a 50/50 (v/v) CO <sub>2</sub> /CH <sub>4</sub> gas mixture. (Stage cut = ratio of permeate to feed flow rate, T = 26 °C, ΔP = 5.5 bar).....	3-13
Figure 3-12 CO <sub>2</sub> permeance and CO <sub>2</sub> /CH <sub>4</sub> separation factor versus feed flow rate for separation of a 50/50 (v/v) CO <sub>2</sub> /CH <sub>4</sub> gas mixture. (T = 26 °C, ΔP = 5.5 bar).....	3-14
Figure 3-13 CO <sub>2</sub> permeance and CO <sub>2</sub> /CH <sub>4</sub> separation factor α as a function of temperature for separation of a 50/50 (v/v) CO <sub>2</sub> /CH <sub>4</sub> gas mixture. (Stage cut =9 %, ΔP = 5.5 bar).....	3-15
Figure 3-14 CO <sub>2</sub> permeance and CO <sub>2</sub> /CH <sub>4</sub> separation factor α as a function of pressure gradient for separation of a 50/50 (v/v) CO <sub>2</sub> /CH <sub>4</sub> gas mixture. (stage cut = 9 %, T = 26 °C). .....	3-16
Figure 3-15 Molecular-sieving behavior of a membrane calcined at 450 °C. The ideal separation factor α <sub>i</sub> represents the ratio of permeance (measured in single-gas permeation tests) for two specified gases.....	3-17
Figure 4-1 Single gas permeance of membranes deposited in the dry nitrogen box and calcined at 300 °C under vacuum (C <sub>6</sub> was used as template for the silica sub-layer). Triangles correspond to 4 different membranes prepared identically, squares correspond to the permeance of the untreated support, the diamonds corresponds to the best results reported before in chapter 3 and is used as standard for comparison.....	4-2
Figure 4-2 Single gas permeance of membranes deposited under clean room condition and calcined at 300 °C under vacuum (C <sub>6</sub> was used as template for the silica sub-layer). Triangles correspond to 4 different membranes prepared identically, squares correspond to the permeance of the untreated support, the diamonds corresponds to the best results reported before in chapter 3 and is used as standard for comparison.....	4-3
Figure 4-3 Comparison of the coating environment: dry nitrogen box (unfiltered Atmosphere) versus class-10 clean room condition. ....	4-5
Figure 4-4 Comparison of the calcination condition: vacuum versus air.....	4-6
Figure 4-5 C <sub>6</sub> -templated dual layer membrane (calcined at 300 °C under vacuum) continuously operated for 150 hours under conditions of constant temperature (T = 26 °C), pressure gradient (ΔP = 5.5 bar), and feed flow rate (345 SCCM).....	4-7
Figure 4-6 Long-term stability of a dual layer membrane. Total time of the experiment was 2 weeks. The numbers correspond to the sequence of permeation measurements. Squares corresponds to room temperature, diamonds to 80 °C.....	4-8

---

Figure 4-7 Step-by-step development of highly selective silica dual layer membranes. Circles corresponds to the untreated 50 Å $\gamma$ -alumina support, triangles to the non-calcined surfactant templated silica sub-layer, squares to the calcined surfactant templated silica sub-layer and diamonds to the microporous selective silica top-layer. ....	4-10
Figure 5-1 Dip-coating over larger pore supports using the same sol as before .....	5-2
Figure 5-2 Setup for aerosol deposition of surfactant-templated silica sols on planar substrates.....	5-3
Figure 5-3 Planar view of a ceramic support before (a) and after (b) aerosol deposition of Brij-56-templated silica sols. ....	5-4
Figure 6-1 Trade-off between selectivity and permeability of polymeric membranes shown at the example of $O_2/N_2$ separation [25]. ....	6-1
Figure 6-2 Comparison of reported membranes for a mixed-gas, $CO_2/CH_4$ separation, (a) present A2**/C6 membrane, vacuum calcined at 300 °C or 450 °C, (b) silica membrane [23] ( $CO_2$ permeance at 100 °C estimated from reported single-component permeation), (c) polyelectrolyte (PVBTAF) membrane [26], (d) polyimide membrane [27], and (e) Zeolite Y membrane [28]. ....	6-2



## LIST OF TABLES

---

Table 1-1 Kinetic diameter of various gases of interest [16].	1-7
Table 2-1 Molar compositions of sols used for silica membrane preparation.	2-2
Table 3-1 The He permeance $F_{He}$ and separation factor $\alpha$ for single and dual layer membranes in comparison	3-2
Table 3-2 Dual layer membrane calcined at 450 °C for separation of a simulated reformat gas mixture (33.98% N <sub>2</sub> , 15.00% CO <sub>2</sub> , 0.997% CO, and 50.023% H <sub>2</sub> ) at 80 °C.	3-18
Table 3-3 Dual layer membrane calcined at 450 °C for separation of a 50/50 (v/v) H <sub>2</sub> /N <sub>2</sub> gas mixture at 80 °C.	3-18
Table 4-1 Ideal selectivity of membranes deposited in the dry nitrogen box (see Figure 4-1).	4-2
Table 4-2 Ideal selectivity of membranes deposited under clean room condition (see Figure 4-2).	4-4



# 1

## INTRODUCTION

---

### 1.1 Inorganic Membranes

Gas separations play important role in the chemical and petrochemical industries and have been traditionally implemented by cryogenic techniques or more recently by adsorption, e.g. pressure swing adsorption (PSA). For example, cryogenic distillation of air is widely used for the production of pure O<sub>2</sub> and N<sub>2</sub>, however this method suffers from high capital investments and intensive energy requirements. Alternatively, PSA is fundamentally useful for separation of a variety of gas mixture based on diffusional or adsorption capacity differences of the mixture components on various molecular sieves such as carbon or zeolites. Although this process is less energy intensive compared to cryogenic distillation, it still suffers from a high degree of complexity since it requires cycling operation between high pressure adsorption and low pressure desorption.

Currently, membrane-based separations attract increasing attention because of the advantages of steady-state operation and low energy requirements. Most commercially used membranes currently are polymeric membranes (e.g. cellulosic derivatives, polysulfone, polyamide, or polyimide membranes). They combine good processability and low production cost which give them high value for commercial application, but they suffer from low thermal, chemical and mechanical stability. Fouling and swelling are common problems that alter membrane properties significantly during operation and drastically reduce their lifetime, primarily for applications involving organic liquids separation.

Inorganic membranes instead have attracted considerable attention for gas, vapor and liquid separations due to their superior thermal, chemical and mechanical stability compared to conventional polymeric membranes. An inorganic membrane system generally consists of a macroporous support providing mechanical strength for an overlying thin, either dense or porous, separation membrane.

Dense inorganic membranes made of palladium or perovskites only allow a specific gas (H<sub>2</sub> or O<sub>2</sub>, respectively) to transport via mechanisms such as solution-diffusion or solid-state ionic conduction. Such membranes require high capital investment due to the use of precious metals and/or extreme synthesis conditions and usually operate reasonably well only under critical conditions, e.g. elevated temperatures. Porous membranes (highly crystalline zeolite as well as amorphous carbon or silica membranes) instead are more attractive since they can be fine-tuned to perform a variety of separations. Theoretically, zeolites are very good candidates for molecular sieving, e.g. separation based on size exclusion, since they possess extremely uniform one-, two- and three-dimensional pores of molecular dimensions which are part of their

crystalline structure. But despite their almost perfect features, preparation of zeolites in membrane form and fine-tuning of their pore size still appear to be difficult tasks at the moment. In addition, zeolites are formed under hydrothermal conditions that impose restrictions in the choice of possible support materials that have to be chemically stable under these highly corrosive synthesis conditions.

Amorphous silica membranes instead, developed and reported here, show many advantages. They combine the narrow pore size distribution offered by crystalline zeolite membranes with the easy processibility of conventional polymeric membranes. Their pore size is tunable in a wide range and they can be processed by a simple dip-coating or spin-coating procedure, which in general is applicable to all types of different support materials, since the support is not exposed to an aggressive chemical environment or extreme temperatures as in the case of zeolite or dense inorganic membranes. In addition, their pore surface can be chemically modified by various ways that are discussed in more detail below.

For porous inorganic membranes to be commercially viable, they must: (a) have small pores with a narrow pore size distribution to allow efficient separation of gases by molecular sieving and (b) be thin enough to allow for high permeation rates in order to maximize productivity. The latter requirement necessitates the use of a supporting carrier substrate that provides mechanical strength to the overlying membrane.

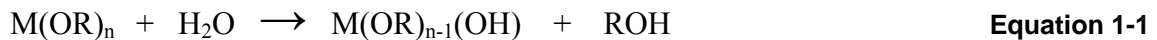
Beside zeolite membranes, commercially available porous inorganic membranes are made from colloidal sols of metal oxides such as  $\gamma$ -Al<sub>2</sub>O<sub>3</sub>, titania and zirconia, typically formed by hydrolysis and condensation of metallorganic precursors in aqueous/alcohol media. The pore size of these sol-gel derived ceramic membranes depends on the primary particle size in the sol (provided that aggregation is avoided, smaller primary particles lead to smaller pores) while the porosity is nearly independent of particle size. Although this concept works well for preparing porous membranes with a pore size down to 40 Å in diameter, problems with cracking occur when the particle size is reduced further to the microporous range (2-10 Å), required for molecular sieving of small gases. In addition, the nanocrystalline ceramic oxides ( $\gamma$ -Al<sub>2</sub>O<sub>3</sub>, TiO<sub>2</sub>, ZrO<sub>2</sub>) used for porous inorganic membrane preparation undergo phase transformations after heating at moderate temperatures that result in undesirable grain growth and subsequent pore size coarsening, implying that these materials are less suitable for development of microporous membranes with molecular sieving capabilities.

Sol-gel processing can overcome the limitations of commercially available porous inorganic membranes by controlling the chemistry of silica sols to produce randomly branched, fractal polymeric sols as opposed to the compact, particulate sols used at the moment. Aggregation, which produces larger pores in particulate sols, can be exploited to our advantage in polymeric sols to actually reduce the pore size via aggregation/ interpenetration and collapse of the fractal polymer clusters during membrane deposition and drying. Through control of the polymer size, the membrane made from these sols spans over the support pores to form a relatively thin, discrete layer with pore openings in the microporous range, dictated by the molecular size of the solvent used (e.g. ethanol or water).

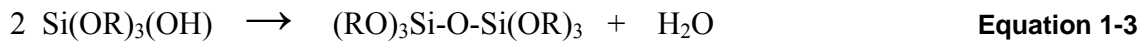
## 1.2 Sol-Gel Processing

### 1.2.1 Sol-gel chemistry

The sol-gel process uses inorganic or metalorganic precursors in aqueous or organic solvents which are hydrolyzed and condensed to form inorganic polymers composed of M-O-M bonds. The most commonly used organic precursors are metal alkoxides  $[M(OR)_n]$ , where R is an alkyl group ( $C_mH_{2m+1}$ ) [2]. Normally the alkoxide is dissolved in alcohol and hydrolyzed by the addition of water under acidic, neutral or basic conditions. Hydrolysis replaces an alkoxide ligand with a hydroxyl ligand:



Condensation reactions involving the hydroxyl ligands produce polymers composed of M-O-M bonds plus, in most cases, the by-products water or alcohol as shown below for silicate condensation:



The reverse of reactions 2 and 3, e.g. siloxane bond alcoholysis and siloxane bond hydrolysis, promote bond breaking and reformation processes that, if extensive, permit complete restructuring of the growing polymer. Silicon alkoxides hydrolyze and condense slowly, so the condensation pathways and condensation rates can be influenced by controlling the sol chemistry, especially by varying the pH,  $H_2O/Si$  ratio or aging time, as reported previously [1]. Basic-catalyzed sols leads to particulate sols, whereas acid-catalyzed sols result in partially condensed, randomly branched polymeric silicates [3]. These polymeric silicates can be characterized by a mass fractal dimension  $D$ , which relates an object's mass  $M$  to its radius  $r_c$  [4]:

$$M \sim r_c^D \quad \text{Equation 1-4}$$

where for mass fractal objects,  $D$  is less than the embedding dimension of space  $d$ ; for our purposes,  $d=3$ . Since in 3 dimensions,  $D < 3$ , the density of mass fractal clusters decreases with the distance from its center of mass:

$$\rho \propto 1 / r_c^{(3-D)} \quad \text{Equation 1-5}$$

Because density is inversely related to porosity, this relationship requires that, unlike Euclidian objects, fractal objects become more porous as their size increase. As shown previously [1, 3] this property can be used to tailor the pore structure of sol-gel derived silica membranes in a range suitable for gas separations.



varying the solvent composition and the fluid/vapor surface tension has a dramatic effect on the porosity of bulk silica gels. For a given sol, this balance between capillary pressure and stiffness of the network depends in turn on the characteristic time scale of the drying process and can be influenced by controlling the atmospheric pressure during drying. For a given drying procedure, the drying of bulk gels occurs slowly over a period of several days due to the long pathways for flow and diffusion, especially if cracking is to be avoided. For films, fast evaporation overlaps the complete deposition process. Within seconds the entrained sol is concentrated and dried to form a thin solid film (typically 10 to 300 nm-thick). This short characteristic time of the thin film deposition represents the time where continuous condensation reactions occur. Thus compared to bulk gels, films are less highly condensed prior reaching the critical point and hence suffer greater collapse during drying. Therefore, films are characterized by smaller pore sizes, lower pore volumes and lower surface areas than their bulk counterparts. By reducing the atmospheric pressure during drying thin films, even higher degree of shrinkage can be achieved, due to reducing the time scale for solvent evaporation, while keeping the condensation rate constant.

### 1.3 Pore size control

Beside the porosity that can be altered by controlling the degree of silicate polymerization as discussed above, porosity can be introduced and tailored by using various different types of templates. In the broadest sense a template may be defined as a central structure around which a network, in our case the silicate network, forms. After removal of the template, cavities are formed which mimic the size and shape of the template used. Various templating methods can be used to tailor the pore size of inorganic membranes. These are solvent templating [5], molecular templating [6] and surfactant templating [7-15].

#### 1.3.1 Solvent and Molecular Templating

The smallest pore size attainable in sol-gel derived silica membranes may be limited by the size of the solvent molecules and/or the alkoxide ligands which remain in the pores after dip coating as well as their hydrolysis products formed by continuous condensation during drying. As generally described above, pores are formed after removal of the solvent during calcination. Since the solvent molecules serve as pore templates, the pore size in membranes prepared from silica sols with different solvents scales with the size of the solvent molecule used (Figure 1-2). Evidence for this effect comes from studies of the kinetic stress relaxation in solvent-substituted silica films calcined at 400°C and exposed to vapors of various sized alcohols [1]. A series of alcohol-substituted acid-catalyzed silica sols were prepared, where methanol, ethanol or isopropanol were substituted for the original ethanol-water pore fluid prior to film deposition. The rate at which capillary stress decreased as the relative pressure was suddenly increased to a particular value was found to decrease in the order of increasing size of the original pore fluid molecules used to prepare the films [1]. This behavior is consistent with an increase in pore size as the size of the substituted solvent molecules increases. By this approach of solvent templating using different alcohols the pore size of sol-gel derived silica membranes can be tailored in a range of ~2.5 to 10 Å, which is the ideal range for

separating small gas molecules. The original water-ethanol mixture as solvent leads to pores of about 3.5 Å (Figure 1-3). Comparing this pore size with the kinetic diameters of various gases of interest (Table 1-1) it is the perfect pore size for various separations, such as CO<sub>2</sub>/CH<sub>4</sub> (the main focus in this research), CO<sub>2</sub>/N<sub>2</sub> or O<sub>2</sub>/N<sub>2</sub> and only small pore size decrease would be necessary for N<sub>2</sub>/CH<sub>4</sub>, which as well is of high industrial interest.

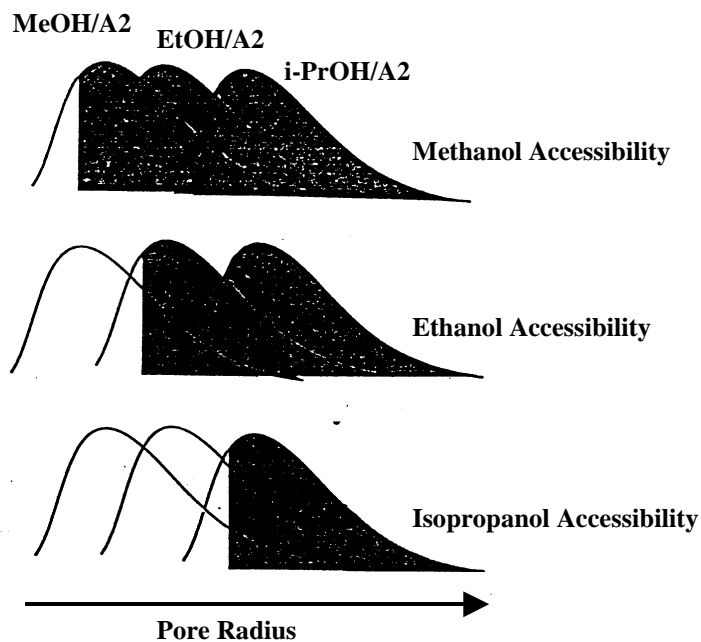


**Figure 1-2**  
Effect of solvent templating on the pore size of sol-gel based silica membranes. ROH/A2 refers to a film prepared from A2\*\* silica sol and solvent substituted by ROH prior dip coating. ROH accessibility refers to the distribution of pore sizes accessible to ROH.

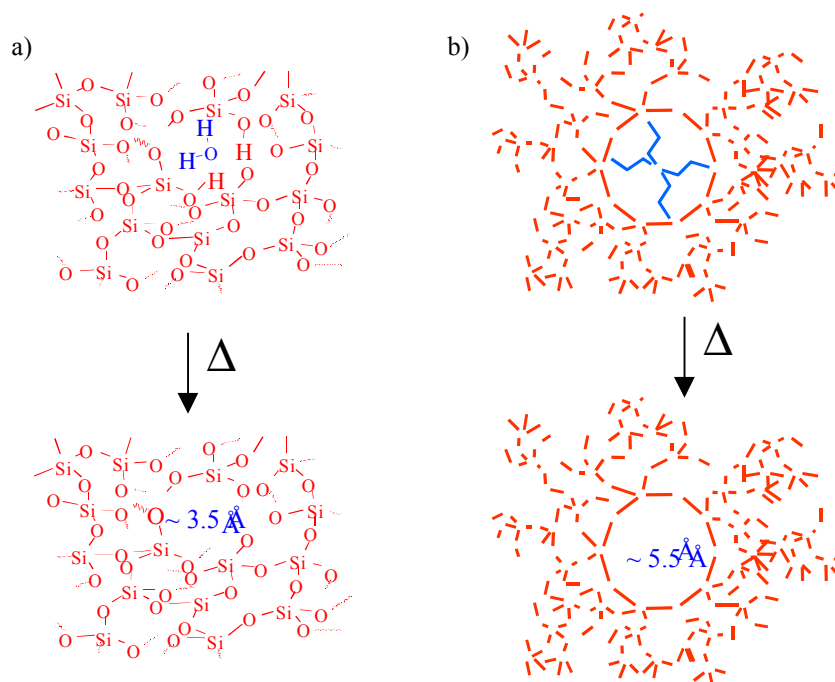


**Figure 1-3**  
Pore size control by a) solvent templating and b) molecular templating.

**Table 1-1**  
Kinetic diameter of various gases of interest [16].

gas molecule	kinetic diameter (Å)
He	2.60
H <sub>2</sub>	2.89
NO	3.17
CO <sub>2</sub>	3.30
O <sub>2</sub>	3.46
N <sub>2</sub>	3.64
CO	3.76
CH <sub>4</sub>	3.80
n-C <sub>4</sub> H <sub>10</sub>	4.30
i-C <sub>4</sub> H <sub>10</sub>	5.00
SF <sub>6</sub>	5.50

Similar to solvent templating, the size of the pores can be tailored by non-reacting organic molecules that are added to the sol used for dip-coating. Funded by a different project this approach was demonstrated by the use of tetrapropylammonium (TPA) [6], a template used commonly in the synthesis of zeolites ZSM-5 or Silicalite-1 (structure code MFI). Using TPA as template the pore size in both zeolite as well as sol-gel derived amorphous silica membranes is  $\sim 5.5 \text{ \AA}$  (Figure 1-3), useful for various organic isomer separations.

### 1.3.2 Surfactant Templating

Surfactants are bifunctional (amphiphilic) molecules that contain a solvent-loving (lyophilic) head group and a solvent-hating (lyophobic) tail. As a result of their amphiphilic nature, surfactants can self-assemble into supramolecular arrays which are held together by interactions such as Van der Waals forces or hydrogen bonding. At concentration above the *critical micelle concentration* (cmc), they form initially spherical or cylindrical micelles or at higher concentrations even periodic hexagonal, cubic or lamellar liquid crystals (Figure 1-4). These supramolecular arrays of organic surfactants can be seen as gigantic templates with diameters in the nanometer range, depending on the length of the tail.

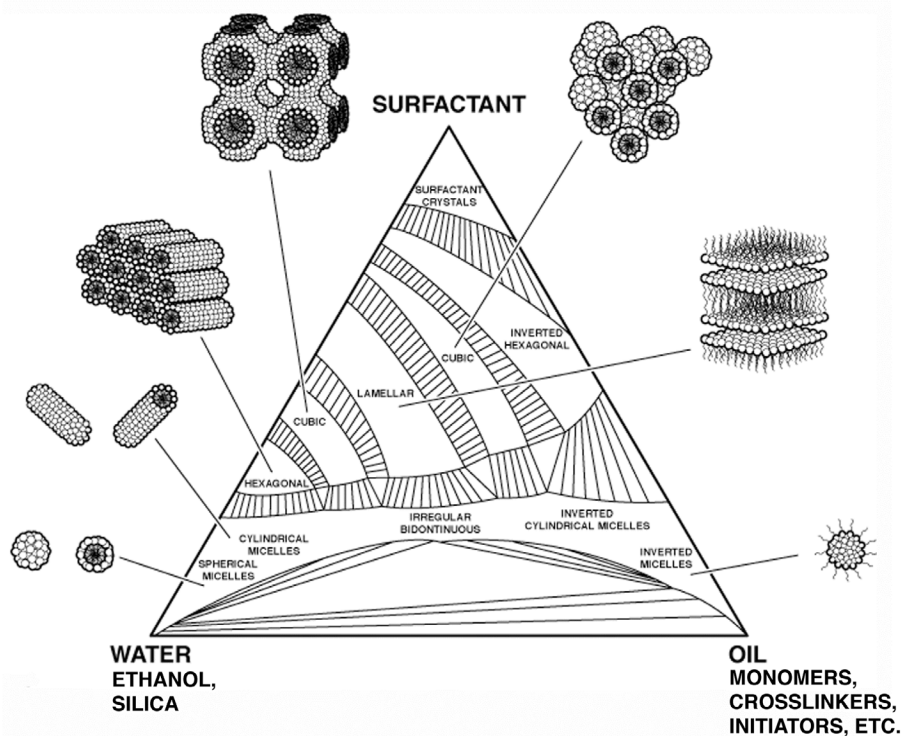


**Figure 1-4**  
Ternary phase diagram of surfactants in water or oil.

By substituting the water solvent surrounding the hydrophilic head groups by silica precursors, silica can be condensed around these self-assembled supramolecular arrays. Thus, after removal of the organic surfactant molecules, pores are maintained which mimic the size, shape and connectivity of the self-assembled liquid crystals (Figure 1-5).

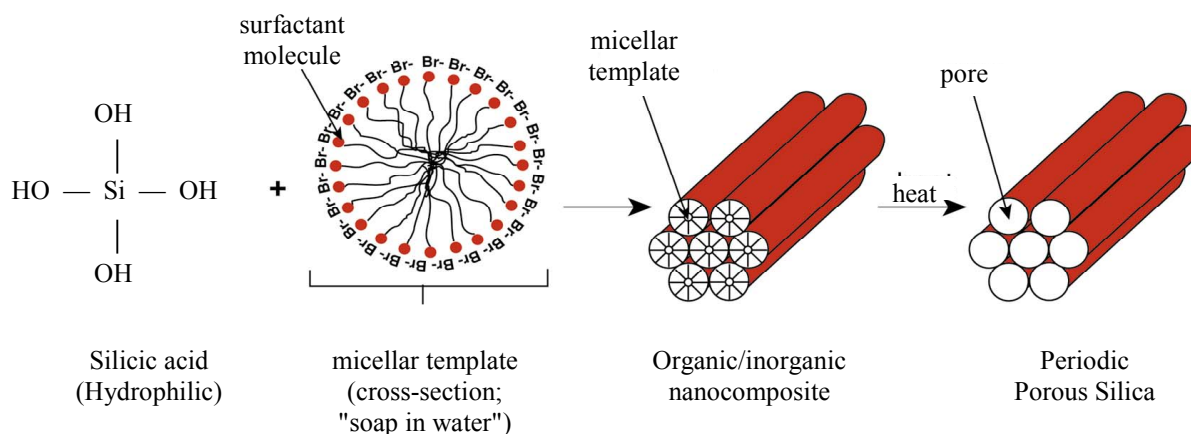


**Figure 1-5**  
Schematic of the liquid crystal templating for formation of mesoporous silica.

Instead of substituting the water solvent with silica precursors, a better approach is to combine self-assembly of surfactants and sol-gel chemistry. Beginning with a homogeneous solution of soluble silica and surfactant prepared in an ethanol/water solvent with a surfactant concentration much below the critical micelle concentration, preferential evaporation of ethanol concentrates the solution in water, non-volatile surfactants and silica species.

The progressively increasing surfactant concentration drives self-assembly of silica surfactant micelles and their further organization into liquid crystalline mesophases [9,10, 13]. Using this scheme during the deposition of the silica membrane by dip-coating (Figure 1-6) the evaporation-induced self-assembly leads to rapid formation of thin film mesophases that are highly oriented with respect to the substrate surface. Through variation of the initial alcohol/water/surfactant mole ratio it is possible to tailor the final structure conserved by the silica condensation.

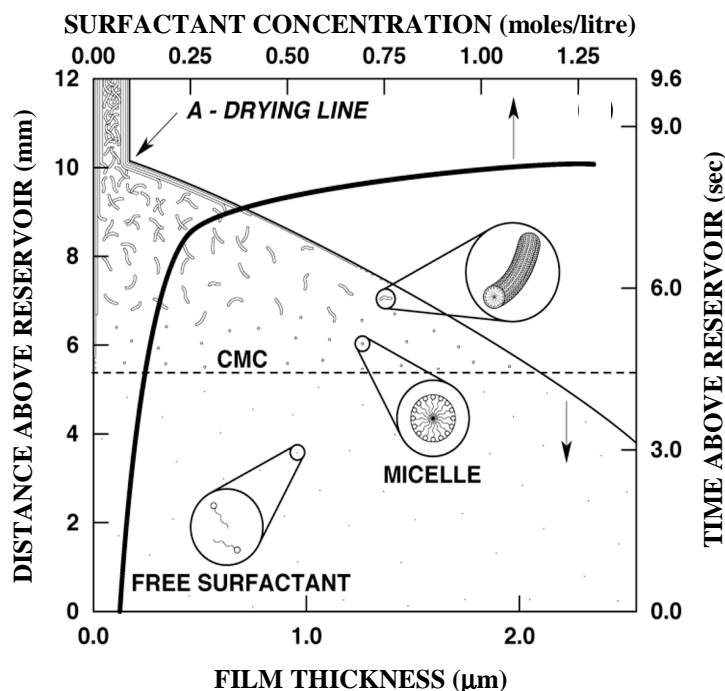


**Figure 1-6**  
Steady state film deposition profile during dip coating surfactant templated silica sol on a porous support.

## 1.4 Objectives

Based on the results achieved previously we focused on the development of sol-gel derived dual-layer silica membranes. In our previous report we mentioned already increasing selectivity by depositing two layers of microporous silica, but by this approach the permeance was reduced by one order of magnitude. The goal in this work was to maintain or even improve the high selectivity and increase the flux at the same time.

The new approach reported here is based on initially depositing an intermediate surfactant-templated mesoporous silica sub-layer which has two functions: (1) it smoothens the surface of the ceramic support material ( $\gamma\text{-Al}_2\text{O}_3$ ) and reduces the degree of defects caused by pinholes due to a rough support surface, without limiting the permeance at the same time, and (2) it avoids deep penetration of the silica sol into the carrier support and therefore enables the deposition of very thin selective microporous silica membrane top-layers.

Furthermore, of high interest in this project was (a) reproducibility of the membrane preparation, (b) effect of the deposition environment, e.g. dry nitrogen atmosphere versus clean room conditions, (c) stability of the membrane performance over a long period of time, (d) possible improvement of selectivity and/or permeance by changing the calcination condition of the mesoporous or microporous silica layer and (e) deposition of the dual-layer membranes onto coarser support materials to increase the permeance and reduce the costs associated with the use of multilayer ceramic supports.

CO<sub>2</sub>/CH<sub>4</sub> separation was the most successful separation in this study. Very high selectivity was found for N<sub>2</sub>/CH<sub>4</sub>. Other separations such as CO<sub>2</sub>/N<sub>2</sub>, CO<sub>2</sub>/NO and He/CH<sub>4</sub> were investigated as well.



# 2

## EXPERIMENTAL

---

### 2.1 Sol Preparation

All silica membranes of the present study were prepared from an A2\*\* sol. Preparation of the A2\*\* sol consists of two acid-catalyzed reaction steps designed to minimize the condensation rates of silica species in order to produce weakly branched polymeric clusters that maximize interpenetration and collapse during film deposition to produce membranes with molecular-sized pores [17]. In the first step, tetraethoxysilane (TEOS), ethanol, water and HCl are mixed in a molar ratio of TEOS: EtOH: H<sub>2</sub>O: HCl = 1.0: 3.8: 1.1:  $5 \times 10^{-5}$  (pH=4.7), refluxed at 60°C for 90 min and cooled to room temperature. We refer to the silicate solution obtained after the first step as *stock sol*, which was used as prepared or stored in a freezer at -20°C. In the second step, additional water and HCl were added to the stock sol and the sol obtained was shaken for 15 min. This silica sol obtained after the second step is referred to as *standard sol* and has a molar composition of TEOS: EtOH: H<sub>2</sub>O: HCl = 1.0: 3.8: 5.0: 0.004 (pH = 2.0).

For the preparation of the sol used for the microporous (solvent-templated) silica membrane, the standard sol was aged at 50°C for 24 h. A dip-coating sol was prepared by diluting the *standard sol* with two times its volume of ethanol.

Surfactant-templated silica sols were prepared using hexyltriethylammonium bromide (C<sub>6</sub>H<sub>13</sub>N(C<sub>2</sub>H<sub>5</sub>)<sub>3</sub>Br, code C<sub>6</sub>), cetyltrimethylammonium bromide (C<sub>16</sub>H<sub>33</sub>N(CH<sub>3</sub>)<sub>3</sub>Br, code CTAB) and Brij-56 (C<sub>16</sub>H<sub>33</sub>(OCH<sub>2</sub>CH<sub>2</sub>)<sub>n</sub>OH, with n~10). Based on previous results, surfactant concentrations were chosen which lead to cubic mesoporous structures (for CTAB and Brij-56). C<sub>6</sub>-surfactant does not lead to ordered structures due to its too small size, but 3-dimensional interconnected porosity is reached by a disordered "worm-like" structure. This structure can be described as bended rods of identical diameters. The surfactant-templated sols were used without aging. The standard sol described above was diluted with ethanol with a volume ratio standard sol/ethanol = 1:2. The surfactants were added prior or after dilution (no difference has been observed if surfactant was added prior or after dilution with ethanol). The surfactant concentration with respect to the diluted standard sol was 0.125 molar (3.6 wt%) for C<sub>6</sub>, 4.2 wt% for CTAB and 4 wt% for Brij-56. The final molar compositions of all sols are summarized in [Table 2-1](#).

**Table 2-1**  
**Molar compositions of sols used for silica membrane preparation.**

dip-coating sol	molar composition					aging
	TEOS	H <sub>2</sub> O	EtOH	HCl	surfactant	
A2**	1.0	5.16	22.27	0.004	0	24 h at 50 °C
C <sub>6</sub> -templated	1.0	5.16	22.27	0.004	0.202	none
CTAB templated	1.0	5.16	22.27	0.004	0.158	none
Brij-56 templated	1.0	4.64	19.74	0.004	0.072	none

All sols were filtered through a 1- $\mu$ m syringe filter (surfactant-templated sols for mesoporous sub-layers) or through a 0.45- $\mu$ m syringe filter (solvent-templated sol for microporous selective top-layer) prior to dip-coating.

## 2.2 Membrane deposition

Membrane supports were prepared by sectioning commercial ceramic tubes (7 mm ID, 10 mm OD) into 5.5 cm-long sections. The supports were then washed twice with ethanol and water in an ultrasonic bath and calcined at 550°C for 1 h in air. Three different types of ceramic tubular supports were used: 1) a 50 Å  $\gamma$ -Al<sub>2</sub>O<sub>3</sub> tube, b) a 200 Å  $\gamma$ -Al<sub>2</sub>O<sub>3</sub> tube and 3) a 0.2  $\mu$ m  $\alpha$ -Al<sub>2</sub>O<sub>3</sub> tube. The 50 Å and 200 Å  $\gamma$ -Al<sub>2</sub>O<sub>3</sub> tubes are asymmetric multilayer tubes formed by coating the inner surface of a coarse-pore  $\alpha$ -Al<sub>2</sub>O<sub>3</sub> tube with successive  $\alpha$ -Al<sub>2</sub>O<sub>3</sub> or  $\gamma$ -Al<sub>2</sub>O<sub>3</sub> layers of decreasing porosity.

Membrane deposition was performed by sol-gel dip-coating. Two different coating environments have been tested, dry nitrogen and class-10 clean room condition. Dry nitrogen environment was achieved using a glove box constantly flushed with a pre-dried nitrogen stream to maintain a relative humidity of 4-6%. Class-10 clean room condition was achieved in a glove box with air circulation at a flow rate of 150 ft/min, which was pre-filtered through a 0.3  $\mu$ m filter. The quality of air in the class-10 clean room condition was measured with a laser-based particle size analyzer before each dip-coating process.

For membrane deposition a support tube was quickly dipped into the sol, soaked in the sol for about 10 sec, withdrawn at a rate of 7.6 cm/min and left drying in the dip-coating box for 15 min. Surfactant-templated silica membranes (mesoporous sub-layers) were vacuum dried at 120°C for 6 h prior to calcination in air to form a dense silica network surrounding the surfactant molecules. For both procedures a heating and cooling rate of 1-2°C/min was employed. The solvent-templated silica membranes (microporous top-layers) were calcined at 300°C for 6 h in vacuum or further at 450°C for 1 h in air (heating and cooling rate 1-2°C/min) without a pre-drying step.

## 2.3 X-ray Diffraction

The structure and possible ordering of surfactant-templated bulk xerogels as well as thin films deposited on Si wafers were analyzed by X-ray powder diffraction, using Ni-filtered  $\text{CuK}\alpha$  radiation and  $\theta$ - $2\theta$  scan mode in reflection geometry. The diffraction patterns were recorded on a Siemens D500 diffractometer and analyzed using the software package JADE. The diffraction patterns were recorded for both the as-deposited as well as the calcined films.

## 2.4 Electron Microscopy (SEM and TEM)

Scanning electron microscopy (SEM) and transmission electron microscopy (TEM) analyses were performed on the cross-sections of films formed on both porous alumina substrates or non-porous Si wafers, to determine thickness, uniformity, defects and morphology of the membrane layers. SEM top views were recorded to determine the surface features and to identify possible crack formation. The samples for SEM were platinum-sputtered and measured with a Hitachi S800 scanning electron microscope. The samples for TEM analysis were sectioned with a diamond wafering saw, ground and polished to a thickness of about  $1\ \mu\text{m}$  and finally ion milled to a thickness of several hundred Å. TEM analysis was performed on a Philips Model CM-30 analytical instrument operated at 300 kV and equipped with a Link energy dispersion spectra analyzer.

## 2.5 Thermogravimetry (TGA/DTA)

Thermogravimetric experiments gave important information on the decomposition temperature of the organic surfactant molecules used to prepare the mesoporous sub-layers as well as the removal and calcination of the non-hydrolyzed remaining alkoxy groups of both solvent- and surfactant-templated sols. Based on the results of TGA, the calcination temperature was chosen for template removal, which is  $450^\circ\text{C}$  for  $\text{C}_6$  and CTAB and  $500^\circ\text{C}$  for Brij-56. TGA/DTA experiments were performed on thin film (petri-dish dried) xerogels using a Polymer Labs Thermal Sciences STA 1500 instrument. About 10-15 mg of sample was heated in air or nitrogen at a heating rate of  $5^\circ\text{C}/\text{min}$ .

## 2.6 Surface Acoustic Wave (SAW) Measurements

The pore structure of bulk gels is determined by isothermal  $\text{N}_2$  or  $\text{CO}_2$  sorption, which measures the mass or volume of gas adsorbed as a function of relative pressure. From the shape of the adsorption isotherm, one can distinguish between non-porous, microporous (pore diameter  $<20$  Å) and mesoporous (pore diameter  $>20$  Å) samples. The surface area and pore size distribution can also be calculated. Due to the very small thickness of the films and membranes ( $<200$  nm), their mass uptake is very small in comparison to bulk powders analyzed by conventional BET.

To address this problem, we employ a thin film characterization technique that uses a surface acoustic wave (SAW) [18-20] device as an extremely sensitive mass detector (sensitivity  $\sim 100$   $\text{pg}/\text{cm}^2$ ). Using the SAW device we can measure the mass of a gas adsorbed in films deposited

on the surface of the SAW substrate as a function of the gas relative pressure. The analysis of these adsorption isotherms is based (as for bulk powder analysis) on the BET theory. Thus, information about the type and size of the pores in a membrane can be inferred from the shape of this isotherm. Surface area is calculated as  $m^2$  of pore area/ $m^2$  of SAW device substrate area, because the thickness of the deposited thin film is generally not known. The pore size of the films can be determined by the adsorption behavior of different-sized probe molecules. Size exclusion would be manifested as a change from a Type I isotherm (characteristic of a microporous surface) to a Type II isotherm (characteristic of a surface which is non-porous to this gas molecule).

Thin film samples were prepared by dip-coating the SAW substrates into silica sols in the same way used for preparation of the supported membranes. The coated and calcined SAW substrates were mounted into a SAW test case. The adsorption isotherms were obtained using a stand-alone unit built and incorporated into a Micromeritics ASAP 2010. The films were outgassed at 150°C under vacuum for 2 h on the ASAP degassing station prior to analysis. Adsorption measurements were made using N<sub>2</sub> at 77 K.

## **2.7 Ellipsometry**

Ellipsometry is used to measure the thickness and refractive index of films deposited on solid supports. Ellipsometry is an optical characterization technique that measures the shifts in the amplitude and phase of a beam of elliptically polarized light when it is reflected from a transparent thin film deposited on a substrate, generally a silicon wafer. When combined, ellipsometry and SAW technique give information about the thickness, surface area, pore volume and pore size of a thin film or membrane. Experiments were performed on a Gaertner model L116C null ellipsometer and a variable angle spectroscopic ellipsometer (VASE) from J.A. Woolam Co. Inc. The % porosity of films was calculated from the measured refractive indices using a Lorentz-Lorenz correlation assuming that all pores are filled with air and using a silica skeleton refractive index value of 1.46.

## **2.8 Water Contact Angle Measurements**

Surface chemistry, especially the hydrophilicity or hydrophobicity, is an important factor for the adsorption properties as well as the stability of a porous membrane. Hydrophobic membrane surfaces are more protected against water attack. A very simple experiment to estimate the surface hydrophilicity or hydrophobicity of a film or membrane is to measure the contact angle of a water droplet sitting on its surface. The equipment used was a VCA-200 system.

## **2.9 Gas Permeation Measurements**

Gas permeation through the tubular silica membranes described in this report was measured using the apparatus shown in [Figure 2-1](#). Ambient moisture can easily condense inside silica micropores, so it is extremely important to evacuate membrane pores via an outgasing procedure prior to the startup of any permeation experiment. The outgasing procedure is conducted at 80°C for at least 3 h under vacuum. The experimental procedure for determining gas permeance

consisted of evacuating both sides of the membrane and then introducing pure gas or mixed gas into the tube side of the membrane. Single-component gases such as He, H<sub>2</sub>, CO<sub>2</sub>, CO, N<sub>2</sub>, NO and CH<sub>4</sub>, and binary or multi-component mixtures were used for testing. The pressure at the tube side (feed) was maintained at a constant level of typically 80 psig. Meanwhile, the pressure at the shell-side (permeate) gradually increased due to permeated gases. Upon exceeding atmospheric pressure, the shell side was opened to ambient pressure. To simulate practical operation, no sweeping gas was used and therefore the problem of a back diffusional flux could be eliminated. The flow rates of all inlet and outlet streams were directly measured by bubble flowmeters. Digital bubble flowmeters (Humonics) were used for low flow rates. High flow rates were measured by using a larger volume bubble flowmeter and a stopwatch. In the extreme case where the permeate flow rate was below the detectable limit of the digital bubble flowmeter (~1 cc/min), the rate of pressure increase at the permeate side was converted to a permeate flow rate.

For mixed-gas permeation measurements, a premixed gas with known composition was used and the compositions of both feed and permeate streams were analyzed as function of time using on-line gas chromatography. The flow rate and feed pressure as well as the temperature of the membrane separator were varied. The experiments were continued until steady-state conditions were reached (no change in flow rates and compositions with time). The change of gas-phase driving force (partial-pressure gradient) of component *i*, Δ*P*<sub>*i*</sub>, along the membrane length was taken into account; therefore, the permeance of the component *i*, *P*<sub>*m,i*</sub>, was defined as

$$P_{m,i} = \frac{J_i}{\Delta P_{ln,i}}$$

$$\text{where } \Delta P_{ln,i} = \frac{(\Delta P_i)^I - (\Delta P_i)^{II}}{\ln\{(\Delta P_i)^I / (\Delta P_i)^{II}\}}$$

where *J*<sub>*i*</sub> was the steady-state flux of component *i* through the membrane; (Δ*P*<sub>*i*</sub>)<sup>I</sup> and (Δ*P*<sub>*i*</sub>)<sup>II</sup> were the partial-pressure differences of component *i* between the feed and permeate pressures of the membrane at the gas entrance (I) and exit (II), respectively.

Separation factors defined by the ratio of permeabilities are equivalent to the ratio of permeances if membrane thickness is identical. Thus, for a single membrane tube, the ideal separation factor α<sub>1</sub> for pure-gas permeation can be defined by the ratio of permeances of individual pure gases. Analogous to the definition of α<sub>1</sub>, the true separation factor α of a mixed gas is defined by the ratio of permeances of the constituent gases.

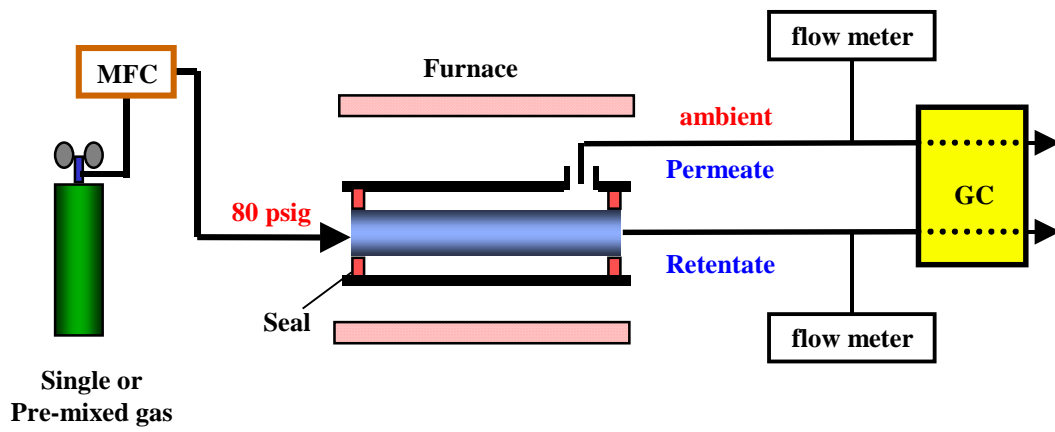


**Figure 2-1**  
Schematic diagram of the experimental setup for gas permeation measurements.

# 3

## DUAL-LAYER MEMBRANES

---

### 3.1 Approach of Dual-Layer Membranes

The two most critical issues of processing porous inorganic membranes are: 1) avoiding defect formation, and 2) controlling pore sizes. For sol-gel derived silica membranes there are three strategies that can be used to avoid or at least reduce defect formation. First, drying-induced stresses as high as 200 MPa in our silica sol system could result in film cracking unless the film thickness is below a critical cracking thickness  $h_c$  [21]. Through adjusting the sol concentration, withdrawal rate of tubular support during dip-coating or sol aging time to maintain the membrane film thickness below the critical cracking thickness  $h_c$  ( $\sim 4000\text{\AA}$  for A2\*\* sol), cracking is avoided. Second, the dip-coating environment can play a crucial role in the quality of the membrane formed. Dust particles deposited on the substrate prior to dip-coating can result in pinhole formation in the membranes. Working under clean-room conditions can reduce the risk of defect formation. Third, the surface roughness of the supporting material has an enormous effect on the formation of defect-free and thin membranes. High surface roughness may result in poor substrate coverage, thus resulting in low selectivities, or may in turn require a thicker membrane to completely cover the substrate surface, resulting in lower permeance of the entire membrane system.

Based on our previous results, there was evidence that a dual-layer membrane structure may improve the membrane performance. This was shown for MTES/TEOS derived silica membranes, see Table 3-1 [1]. By dip-coating a second layer of silica sol an enormous increase in selectivity has been observed. Despite the improvement in selectivity the permeances of even small gases like He were dramatically decreased by more than one order of magnitude. The increase in selectivity clearly shows that the first layer is relatively defective, probably due to the surface roughness of the underlying support tube. This first silica layer smoothens the support surface and therefore facilitates the second layer to be defect-free. Furthermore, due to the smaller pore size of the first silica layer in comparison to the  $50\text{\AA}$   $\gamma\text{-Al}_2\text{O}_3$  support, the silica sol will not deeply penetrate during the dip-coating of the second silica layer.

**Table 3-1**  
**The He permeance  $F_{\text{He}}$  and separation factor  $\alpha$  for single and dual layer membranes in comparison**

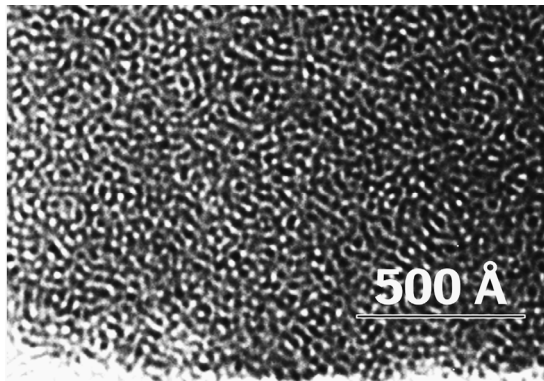
MTES/TEOS membrane	$F_{\text{He}}$ ( $\text{cm}^3/\text{cm}^2 \text{ s cmHg}$ )	$\alpha$ (He/N <sub>2</sub> )	$\alpha$ (He/SF <sub>6</sub> )	kinetic diameter (Å)		
				N <sub>2</sub>	He	SF <sub>6</sub>
1 layer	$2.4 \cdot 10^{-2}$	1.6	3.9			
2 layers	$1.3 \cdot 10^{-3}$	17.1	240	3.64	2.6	5.5

The goal in this study therefore was to use a dual-layer approach that results in improved selectivity by forming an asymmetric silica membrane. The first silica sub-layer was intended to only improve the surface finish of the support material without significantly reducing its permeability. By choosing sols that lead to pore sizes in intermediate range between the ceramic tubular support (50 Å) and the selective silica membrane top-layer (average pore size ~3.5 Å), further penetration into the underlying support or silica layer can be reduced. In this way, the actual thickness of the selective microporous top-layer can be decreased which should lead to an increased flux through the final membrane.

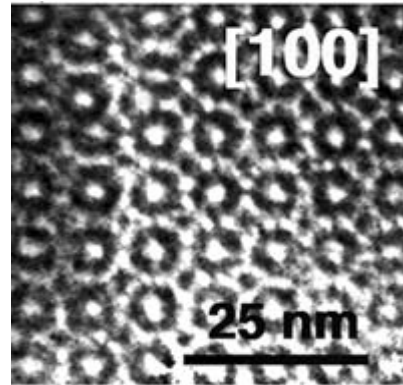
### 3.2 Surfactant-Templated Silica

To form a mesoporous silica sub-layer, surfactant templating was used with surfactants leading to pore sizes in the range of 10-35 Å and a 3-dimensional interconnected pore structure, to ensure diffusion perpendicular to the substrate surface. The surfactant-templated silica sub-layer is designed with both high porosity (~50 vol%) and low tortuosity to avoid creating additional flow resistance. Surfactants used for this approach were C<sub>6</sub> (hexyltriethylammonium), CTAB (cetyltrimethylammonium) and Brij-56.

As known from previous investigations, CTAB [13] and Brij-56 can form a cubic mesoporous silica phase (Figure 3-1) if used in the proper concentration range. C<sub>6</sub> instead has a too short tail to self-assemble an ordered structure. But nevertheless, a disordered "worm-like" structure is formed (Figure 3-1) which consists of a 3-dimensional interconnected pore system and thus ensures transport perpendicular to the substrate surface. As will be shown later, the identical structures and pore sizes have been found for surfactant templated silica thin films and membranes.



- C<sub>6</sub>** - randomly oriented cylindrical pores  
 - pore size 10 - 12 Å  
 - porosity > 30 %



- CTAB** - cubic structure (4.2% CTAB)  
 - pore size 18 - 20 Å  
 - porosity 40 - 60%  
**Brij-56** - cubic structure (4 wt% Brij-56)  
 - pore size 25 - 30 Å  
 - porosity 40 - 60 %

**Figure 3-1**  
**Transmission electron micrographs of C<sub>6</sub> and CTAB templated silica gels.**

To find suitable conditions to remove the surfactants used to template the silica network, thermogravimetric investigations were carried out on silica xerogels prepared with the identical sols used for membrane preparation. Bulk xerogels were prepared by drying thin layers of silica sols on petri-dishes under ambient conditions. Figure 3-2 shows the result of as-prepared C<sub>6</sub>-surfactant-templated silica bulk xerogel heated slowly with 2°C/min in air. The differential thermal analysis (DTA) curve showed an endothermic peak near 200°C corresponding to the beginning of a drastic weight loss, indicating the decomposition of the C<sub>6</sub>-surfactant template. At about 350°C and a weight loss of about 45%, an exothermic peak indicated the oxidative pyrolysis of surfactant and residual organics as well as the condensation products ethanol and water from temperature-induced silica condensation. Between 350-500°C only little more weight loss was observed and at temperatures above 500°C up to the highest temperature measured (973°C), the mass of the sample did not change significantly anymore.

Similar results were observed for the CTAB and Brij-56 templated silica xerogels. The major mass loss was found to occur at temperatures below 450°C, attributed to the decomposition and oxidation of the organic surfactant molecules and silica condensation products. Total removal of the organic surfactant molecules was indicated by the white powder obtained after the thermogravimetric experiments. Since all three surfactants chosen for templating mesoporous silica sub-layers are totally removed by heating at 450°C, this temperature was used as the calcination temperature for the mesoporous surfactant-templated silica sub-layers.

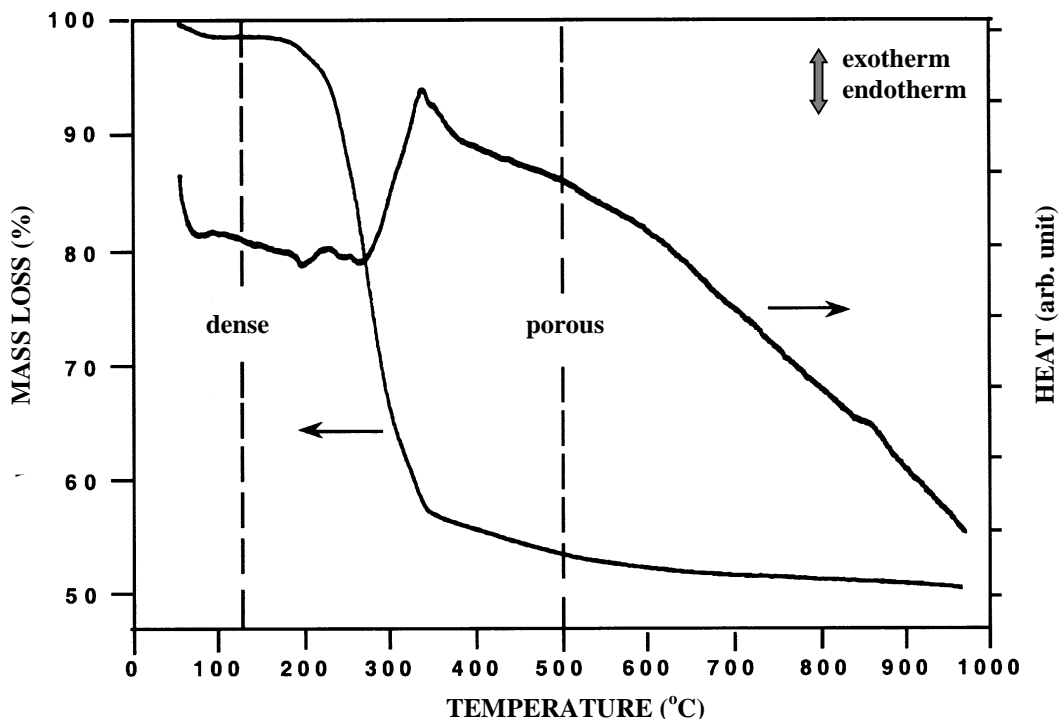


**Figure 3-2**  
**Thermogravimetric analysis (TGA/DTA) of  $C_6$  templated silica xerogel in air at a heating rate of  $2\text{ }^\circ\text{C}/\text{min}$ . The dashed lines indicate the calcination temperatures used to prepare materials for nitrogen adsorption and gas permeation measurements.**

As mentioned earlier, the surfactants self-assemble during the dip-coating process as a result of ethanol evaporation. The silica arranges itself at the same time around these supramolecular arrays of surfactant molecules. Initially the silica species are little condensed and can still rearrange. To prevent the collapse of the pores during removal of the surfactant molecules, the silica network around has to be stiff, e.g. condensed to a certain degree. Furthermore, the final pore size of the network should be determined by the size and shape of the self-assembled surfactant molecules. The silica network surrounding the surfactants, or the pores after their removal, should be as dense as possible. As discussed before, densification of the silica network can be achieved by drying the silica/surfactant thin films under vacuum at moderate temperature that is far below the surfactant calcination temperature. In this way, the shrinkage of the silica network is enhanced due to accelerated solvent evaporation. Condensation instead occurs as well, but with unchanged rate. Thus, the silica network is shrunk, densified, and due to ongoing condensation, is stabilized around the surfactant molecules prior to their removal. Therefore, for the membranes reported in this study, the surfactant-templated mesoporous silica sub-layers were pre-dried in vacuum at  $120\text{ }^\circ\text{C}$  for 6 h prior to calcination at  $450\text{--}500\text{ }^\circ\text{C}$  for 3 h in air. In both steps, heating and cooling rates were  $1\text{--}2\text{ }^\circ\text{C}/\text{min}$ . The pure white color of the membranes was taken as an indication for total removal of all organic residues in the silica layer as well as in the ceramic supporting tube.

The average pore size, pore size distribution and surface area of the surfactant- templated silica was investigated by surface acoustic wave (SAW) technique. As described before, this technique can measure very little mass uptake and therefore is ideal for measuring adsorption isotherms of thin porous films. The films on the SAW devices are prepared from the same sol used above for the thermogravimetric studies and were dip-coated under conditions identical to those employed for the supported silica membranes. The N<sub>2</sub> sorption isotherm of the C<sub>6</sub>-templated silica thin film (calcined 1 h at 500°C and outgased under vacuum prior to measurement) appeared to be of Type I, characteristic of microporous materials (Figure 3-3). CTAB-templated silica thin film instead appeared to be of Type II without hysteresis, characteristic of mesoporous materials. Brij-56 templated silica thin film (not shown) showed similar behavior as CTAB. A Type II N<sub>2</sub> sorption isotherm was found, indicating mesoporosity. Based on a density functional theory (DFT) model, average pore diameters of the C<sub>6</sub>- and CTAB-templated silica were calculated at around 10-12 Å and 18-20 Å, respectively, with a narrow pore size distribution, which is consistent with TEM observations shown above. Furthermore, the surface area and porosity of the C<sub>6</sub>-templated silica, calculated from the N<sub>2</sub> sorption isotherms, were 575 m<sup>2</sup>/g and 28%, respectively. Porosity determined by ellipsometry agreed well with the result calculated from the N<sub>2</sub> sorption isotherms. A more detailed characterization of the CTAB-templated silica is reported by Sehgal and Brinker [5].

N<sub>2</sub> sorption isotherms of calcined A2\*\* xerogel appeared to be Type I with a very sharp increase of N<sub>2</sub> volume adsorbed within a relative pressure of 0 to 0.01 (Figure 3-3), indicating a small pore size and narrow pore size distribution. The corresponding thin film instead characterized using the SAW-based technique (data not shown) indicated no sorption of N<sub>2</sub> at 77 K but showed a Type-I sorption isotherm of CO<sub>2</sub> at dry ice temperature. This shows that the thin silica films are microporous, as expected, but with a smaller pore size than the bulk silica xerogels prepared using the same sol. These differences in pore size are attributed to differences in drying rates. Rapid drying of films avoids siloxane condensation, promoting the collapse of the silica network by the capillary stress [18]. More detailed characterization of A2\*\* was reported in our last report [1] and more recently by Lu et al. [13].

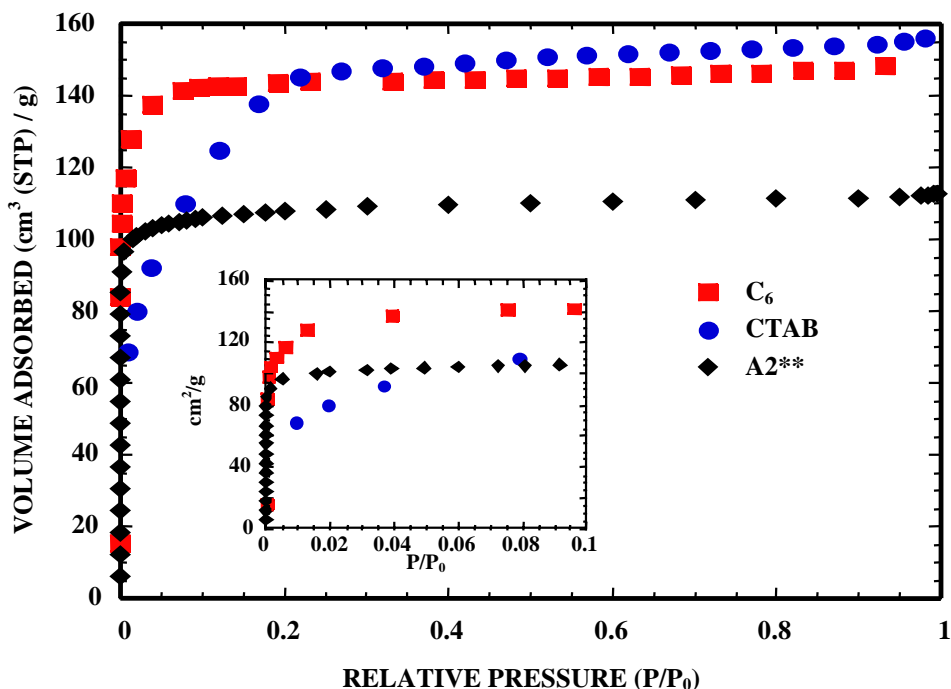


**Figure 3-3**  
Nitrogen adsorption isotherm (77K) of both thin silica films (C<sub>6</sub> and CTAB templated) and bulk silica xerogel (A2\*\*) after removal of templates by calcination at 500 °C in air.

### 3.3 Dual-Layer Membranes

Dual-layer membranes were prepared by subsequent dip-coating of: 1) the surfactant-templated silica sol and, after drying and calcination, 2) the solvent-templated A2\*\* silica sol. To remove any big particles formed in the sols, both sols were filtered prior to dip-coating. The surfactant containing sols were filtered with a 1  $\mu\text{m}$  syringe filter, while the A2\*\* sol was filtered through a 0.45  $\mu\text{m}$  syringe filter. Both silica layers were dip-coated in a laminar flow (150 ft/min) chamber under class-10 clean-room conditions. The sol pre-filtering step apparently prevented membranes from foreign-particle contamination during processing. One could imagine that 1  $\mu\text{m}$  foreign particles could easily penetrate through the thin selective top-layer ( $\sim 30$  nm), resulting in pinholes. As the selective top-layer becomes thinner and thinner, such contamination control becomes even more crucial.

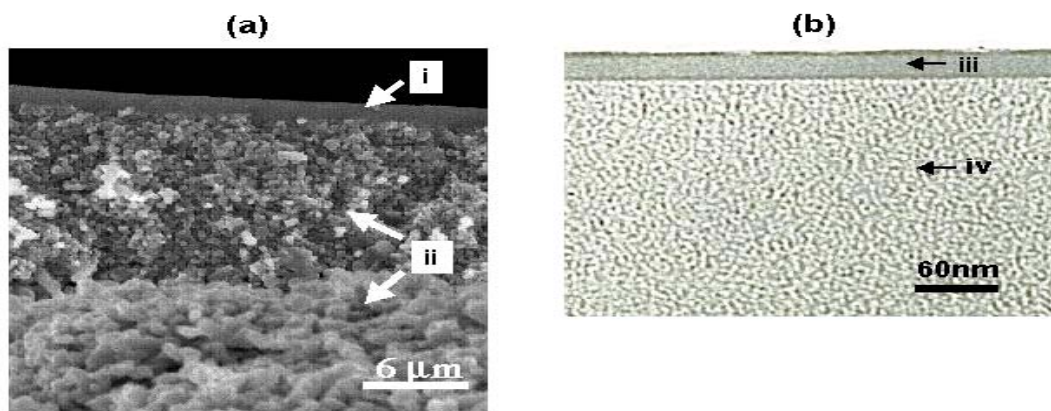


**Figure 3-4**  
**Cross-sectional electron micrographs of an asymmetric membrane: (a) SEM overview- (i)  $\text{SiO}_2$  membrane (see (b) in details) on top of  $\gamma\text{-Al}_2\text{O}_3$  layer, (ii) asymmetric  $\alpha\text{-Al}_2\text{O}_3$  support, and (b) TEM micrograph revealing the dual-layer silica membrane- (iii)  $\text{A2}^{**}$  top layer, (iv)  $\text{C6STS}$  sub-layer**

This two-step coating procedure resulted in tubular membranes with gradual changes of pore size from  $50 \text{ \AA}$  (inner surface of commercial  $\gamma\text{-Al}_2\text{O}_3$  support) to  $10\text{-}12 \text{ \AA}$ ,  $18\text{-}20 \text{ \AA}$  or  $25\text{-}30 \text{ \AA}$  for the  $\text{C}_6$ -, CTAB- or Brij-56-templated mesoporous silica sub-layer, respectively, and further to  $3\text{-}4 \text{ \AA}$  (microporous  $\text{A2}^{**}$  silica top-layer). Electron micrographs revealed the cross-section of an asymmetric supported membrane (Figure 3-4). The porosity difference between the overlying microporous silica membrane ( $\text{A2}^{**}$ ) and the  $\text{C}_6$  surfactant-templated mesoporous silica sub-layer results in contrast differences. Thus, the thin ( $\sim 30 \text{ nm}$ ) microporous top-layer can be clearly distinguished from the underlying mesoporous sub-layer. Furthermore, it can be seen that the  $\text{C}_6$ -templated silica sub-layer shows the same randomly oriented worm-like structure as observed and discussed before for the bulk xerogels. The SEM top-view of the  $\text{A2}^{**}$  membrane layer (Figure 3-5) was featureless, suggesting a defect-free surface.

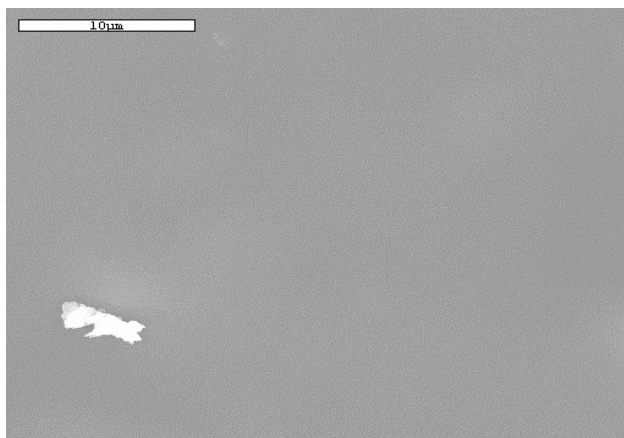


**Figure 3-5**  
**SEM top-view of a dual layer membrane with  $\text{C}_6$ -templated silica sublayer.**

Similar as described before for the surfactant-templated silica, the pore size and stability of the pore structure of the solvent-templated silica membrane is affected by the treatment of the membrane after dip-coating. Slow heating to the final calcination temperature ensures siloxane condensation and densification around the solvent templating molecules. Therefore, the A2\*\* membrane layer was heated under vacuum at a heating rate of 1-2°C/min from room temperature to 300°C for 6 h to evaporate the solvent and promote further pore shrinkage. The vacuum calcination procedure also resulted in the decomposition of surface ethoxy groups, creating a surface deposit of amorphous carbon (visible as a black coating). This coke formation on the membrane surface changes the surface chemistry of the silica membranes. Usually amorphous silica is highly hydrophilic due to the large amount of terminal silanol groups. The carbon coating instead leads to a highly hydrophobic pore surface, which caused an increase in the water contact angle from 17° to 41°. This high degree of hydrophobicity may protect the membrane from water attack and contribute to an improved hydrothermal stability which is necessary for increased membrane life-time.

### **3.4. Comparison of Membranes With and Without Sub-layer**

Silica has long been known to exhibit reversible CO<sub>2</sub> adsorption at room temperature [3]. Therefore, for the separation of CO<sub>2</sub> from other weakly adsorbing gases (e.g. O<sub>2</sub>, N<sub>2</sub>, CH<sub>4</sub>) using silica membranes, one can expect an additional CO<sub>2</sub> surface flow at lower temperatures. In addition, preferential CO<sub>2</sub> adsorption inside micropores at low temperatures may enhance CO<sub>2</sub> selectivity due to the concomitant reduction of the pore aperture for weakly adsorbing gases. This phenomenon was also observed for a zeolitic membrane where great differences between mixed-gas and single-gas permeation were measured due to preferential CO<sub>2</sub> adsorption [22]. In these cases, mixture separation factors strongly depend on feed composition and cannot be directly predicted by single-gas permeation under low-temperature operating conditions.

The surfactant-templated silica sub-layer may serve to: (1) eliminate intrinsic defects on porous supports and promote pore uniformity; therefore, increasing selectivity, and (2) prevent a subsequently deposited microporous top-layer from deeply penetrating into the support (the polysilicic clusters of the A2\*\* sol are larger than the pore size of surfactant-templated silica sub-layers), thus enhancing flux. For membranes with only a C<sub>6</sub>-, CTAB- or Brij-56-templated sub-layer (without the microporous top-layer), gas transport occurred by Knudsen diffusion, as determined by the probe gases used (He, H<sub>2</sub>, CO<sub>2</sub>, N<sub>2</sub> and CH<sub>4</sub>). In contrast, for the dual-layer membrane, the microporous top-layer was capable of discriminating gas molecules such as He (2.6 Å), H<sub>2</sub> (2.89 Å), CO<sub>2</sub> (3.3 Å), N<sub>2</sub> (3.64 Å) and CH<sub>4</sub> (3.8 Å) via molecular sieving (see further discussion below). We also compared a single-layer microporous membrane (without a surfactant templated sub-layer) to the dual-layer membrane (Figure 3-6 and Figure 3-7). At 60°C, the dual-layer membrane exhibited four-fold higher CO<sub>2</sub> permeances and four-fold higher CO<sub>2</sub>/CH<sub>4</sub> selectivity than the single-layer membrane for pure gas permeation. For the dual-layer membrane, ideal separation factors of various gas pairs (e.g.  $\alpha_i(\text{CO}_2/\text{CH}_4) = 102$  at 25°C) largely exceeded Knudsen separation factors (e.g.  $\alpha_K(\text{CO}_2/\text{CH}_4) = 0.6$ ).

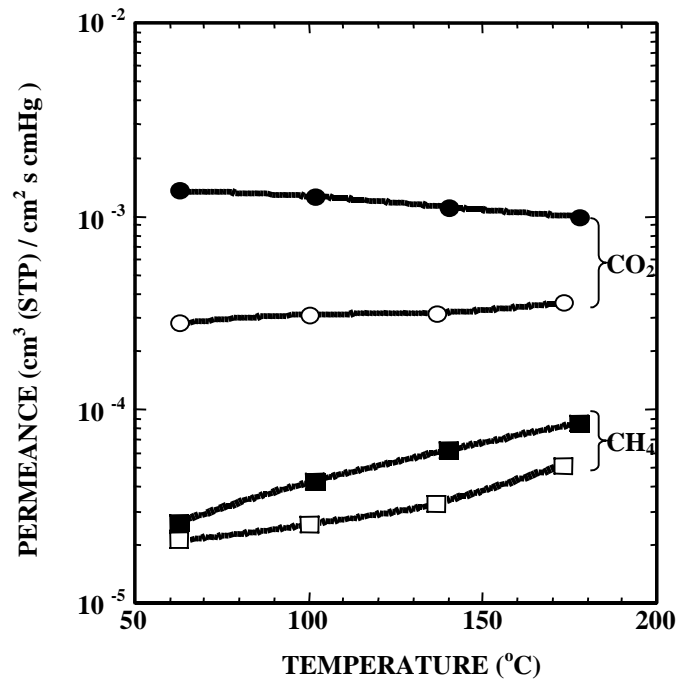


**Figure 3-6**  
Comparison of gas permeances of the microporous membrane (A2\*\*) with and without a C<sub>6</sub>-templated sub-layer. (solid symbols correspond to dual layer membranes, open symbols correspond to single layer membrane without sub-layer).

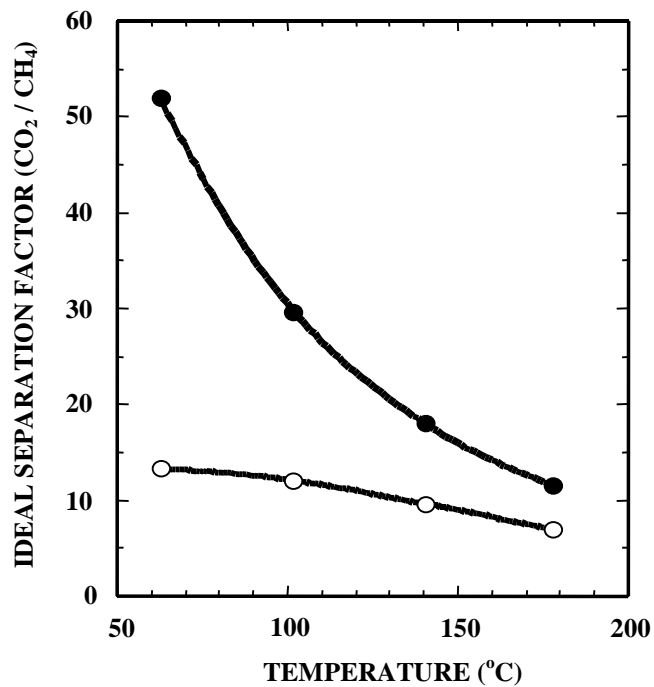


**Figure 3-7**  
Comparison of selectivity of the microporous membrane (A2\*\*) with and without a C<sub>6</sub>-templated sub-layer. (solid symbols correspond to dual layer membranes, open symbols correspond to single layer membrane without sub-layer).

For microporous gas diffusion, permeance is proportional to  $\exp(-E_a/RT)$  under conditions maintaining a constant pressure gradient across the membrane, where  $E_a$ ,  $R$ , and  $T$  are activation energy, gas constant and temperature, respectively [23]. In Figure 3-6 and 3-7 for the dual-layer membrane, the negative activation energy of  $\text{CO}_2$  permeation ( $E_a=-3.37$  kJ/mol) under a constant pressure gradient ( $\Delta P=5.5$  bar) indicated the occurrence of  $\text{CO}_2$  capillary condensation, where  $\text{CO}_2$  transported with high density through narrow pores at lower temperatures. On the contrary,  $\text{CO}_2$  capillary condensation was less significant for the single-layer membrane; therefore, a gradual increase in  $\text{CO}_2$  permeance with temperature (activated transport) was observed ( $E_a=2.48$  kJ/mol). Moreover, the activation energy of  $\text{CO}_2$  was much lower than that of  $\text{CH}_4$ . The activation energy of  $\text{CH}_4$  transport was 9.64 kJ/mol for the single-layer membrane and 12.92 kJ/mol for the dual-layer membrane. This showed that  $\text{CH}_4$  diffused through the membrane mainly via activated transport. This also suggested that, compared to single-layer membranes, dual-layer membranes exhibit a much narrower pore-size distribution. The combination of the  $\text{CO}_2$  condensation effect and  $\text{CH}_4$  activated transport can well explain the drastic increase in ideal separation factor of  $\text{CO}_2/\text{CH}_4$  upon decrease in temperature, particularly for the dual-layer membrane (Figure 3-7).

This sub-layer effect was demonstrated in other surfactant-templated systems as well. Mesoporous CTAB-templated silica sub-layers showed the same effect as the microporous  $\text{C}_6$ -templated silica sub-layer. A new approach was developed to prepare a continuous mesoporous, surfactant-templated silica sub-layer as support of a subsequently deposited microporous membrane. A commercial 50 Å  $\gamma\text{-Al}_2\text{O}_3$  membrane tube was dip-coated into the CTAB-templated silica sol followed by drying and calcination to remove the surfactant template. The membrane was further dipped into a (bis(triethoxysilyl)ethane) (BTE) silica sol, prepared by mixing BTE and TEOS (tetraethoxysilane) together with ethanol,  $\text{H}_2\text{O}$  and  $\text{HCl}$  in a molar ratio of 0.8: 0.2: 3.8: 5.1:  $5.3 \times 10^{-3}$ . The ethane ligands ( $-\text{CH}_2\text{CH}_2-$ ) of the BTE embedded in the silica framework were removed by calcination at 280°C for 3 h, creating micropores. A comparison of the membranes with and without a mesoporous sub-layer is shown in Figure 3-8 and 3-9. Results again suggested that dual-layer membranes with a mesoporous sub-layer exhibit higher permeance and better selectivity than the single-layer membrane without a sub-layer. This consistent behavior implied the crucial role of the sub-layer in improving both the flux and selectivity of an overlying microporous silica membrane.

Similar result was found with molecular-templated silica membranes (not shown here), whose research was funded from a different project. The selective silica top-layer in these membranes was templated with tetrapropylammonium as molecular template [24]. Its pore size after calcination is significantly larger ( $\sim 5.5$  Å) than the water/ethanol solvent-templated silica of interest in this project. But nevertheless, we found that  $\text{C}_6$ - or CTAB-templated silica sub-layers improve both permeance as well as selectivity for those membranes as well.

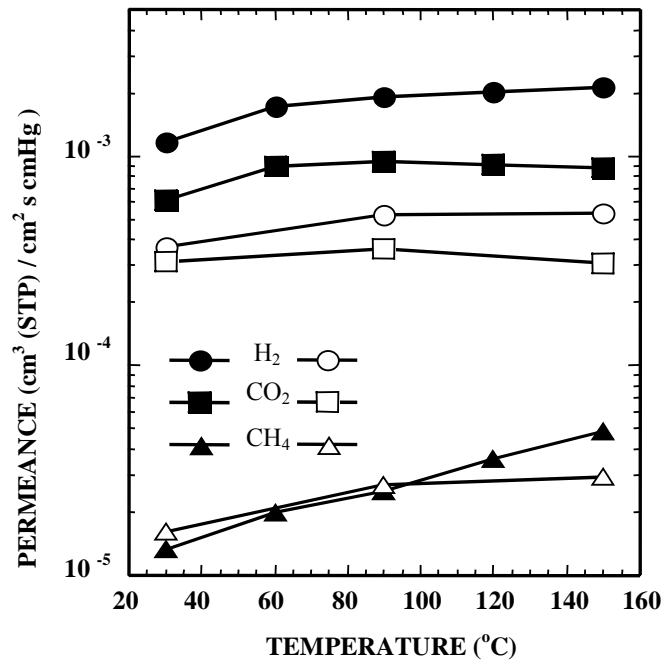


**Figure 3-8**  
Comparison of gas permeances of a BTE/TEOS membrane with and without a mesoporous CTAB-templated sub-layer. (solid symbols correspond to dual layer membranes, open symbols correspond to single layer membrane without sub-layer).

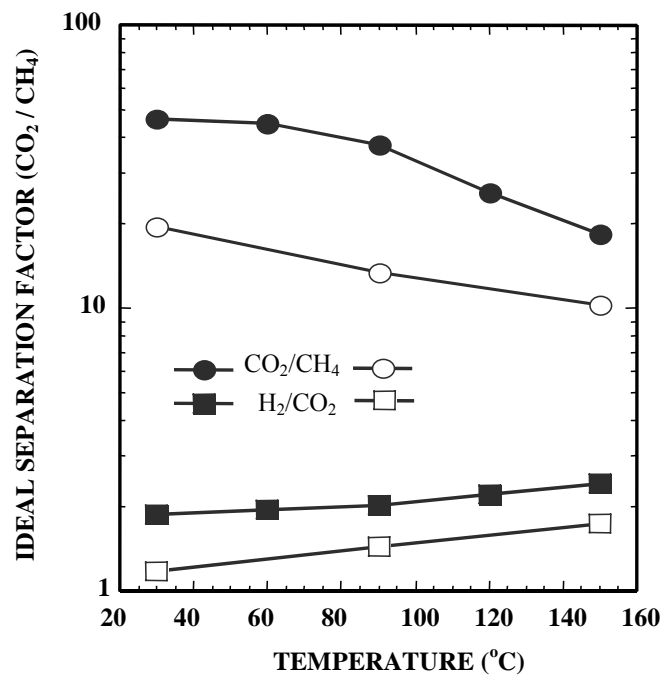


**Figure 3-9**  
Comparison of selectivity of a BTE/TEOS membrane with and without a mesoporous CTAB-templated sub-layer. (solid symbols correspond to dual layer membranes, open symbols correspond to single layer membrane without sub-layer).

Furthermore, the same concept has been extended to the use of an ordered mesoporous silica membrane as a sub-layer to minimize transport resistance. For example, a nonionic block copolymer surfactant Brij-56 was used as a structure-directing agent in place of the previously discussed ionic surfactants, e.g. C<sub>6</sub>- and CTAB. The Brij-56 surfactant-templated silica shows both high porosity (64%) and an ordered cubic structure (uniform pore size ~25-30 Å) and is therefore a promising candidate for use as a sub-layer for a subsequently deposited microporous membrane, as shown in [Figure 3-10](#) as dual-layer coating on a silicon wafer. And as has been shown in this study (not shown graphically), similar results were obtained with Brij-56 templated silica sub-layer. Both permeance and selectivity were significantly improved in a Brij-56 templated dual-layer silica membrane in comparison to a single-layer membrane.

No significant difference has been observed in the performance of these three different dual-layer membranes prepared and investigated in this study.

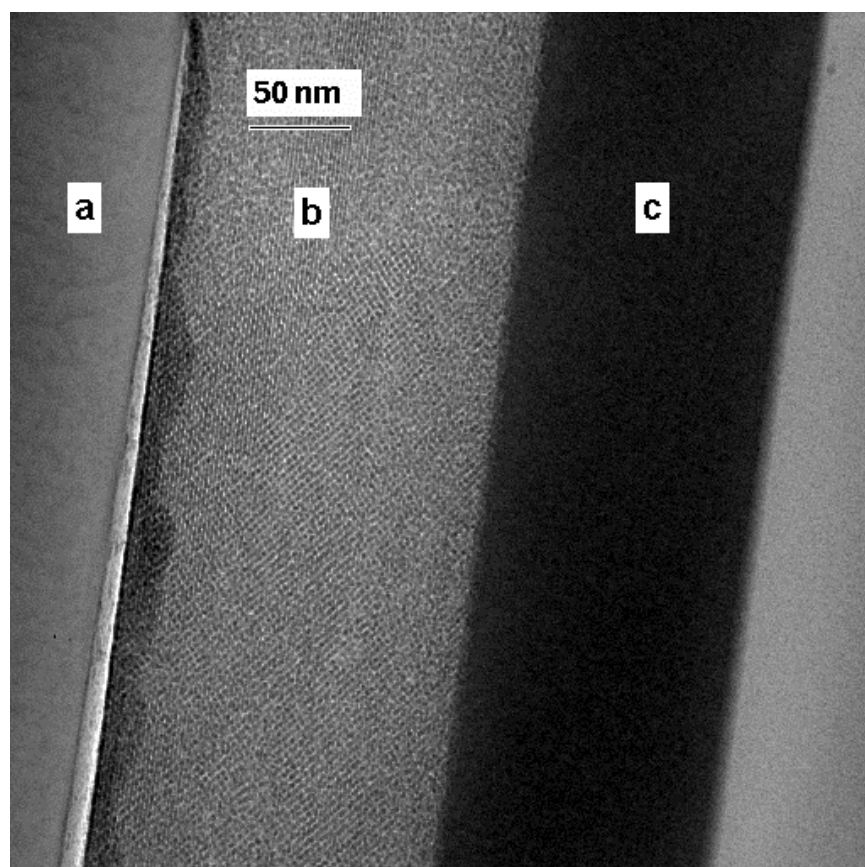


**Figure 3-10**  
TEM cross-sectional electron micrograph of a dual-layer micro-porous silica membrane on top of a silicon wafer, (a) silicon wafer, (b) ordered cubic mesoporous silica film templated by Brij-56 block-copolymer surfactant and (c) microporous layer (A2\*\*).

### 3.5 Effect of Feed Flow Rate, Temperature and Pressure Gradient

The effect of temperature, feed flow rate and pressure gradient across the dual-layer membrane prepared with a C<sub>6</sub>-templated silica sub-layer and calcined in vacuum at 300°C, on both the CO<sub>2</sub> permeance and CO<sub>2</sub>/CH<sub>4</sub> separation factor was investigated with mixed-gas permeation experiments under steady-state conditions. The feed used was a 50/50 (v/v) CO<sub>2</sub>/CH<sub>4</sub> mixture.

For the investigation of the feed flow-rate effect, experiments were performed at constant temperature (26°C) while maintaining a constant pressure gradient across the membrane ( $\Delta P = 5.5$  bar) (Figure 3-11 and 3-12). The stage cut  $\theta$  is defined as the ratio of permeate to feed flow rate and represents the fraction of feed gas permeated through the membrane.  $\theta$  is increased by decreasing the feed flow rate, but at the expense of the purity of CO<sub>2</sub> recovered at the permeate side (Figure 3-11). At a high feed flow rate (low stage cut), the concentration of the fast permeating gas, CO<sub>2</sub>, remained high at the retentate side; therefore, a high CO<sub>2</sub> driving force across the membrane was maintained. This allowed CO<sub>2</sub> molecules to pass through the membrane pores with maximal driving force and less hindrance by larger CH<sub>4</sub> molecules (Figure 3-12). This also indicated that flux and separation factor were a strong function of retentate compositions in the mixed-gas mode. The CO<sub>2</sub> permeance can reach values as high as  $3 \times 10^{-4}$  cm<sup>3</sup>(STP)/(s-cm<sup>2</sup>-cm-Hg), while the CO<sub>2</sub>/CH<sub>4</sub> selectivity,  $\alpha(\text{CO}_2/\text{CH}_4)$ , can reach values up to 200 by increasing the feed flow rate.

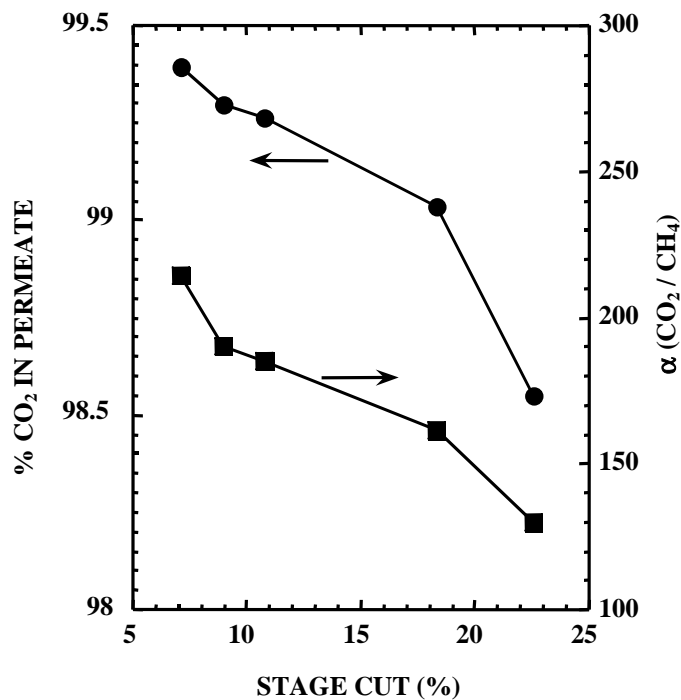


**Figure 3-11**  
%CO<sub>2</sub> in permeate and CO<sub>2</sub>/CH<sub>4</sub> separation factor versus stage cut for separation of a 50/50 (v/v) CO<sub>2</sub>/CH<sub>4</sub> gas mixture. (Stage cut = ratio of permeate to feed flow rate, T = 26 °C,  $\Delta P = 5.5$  bar).

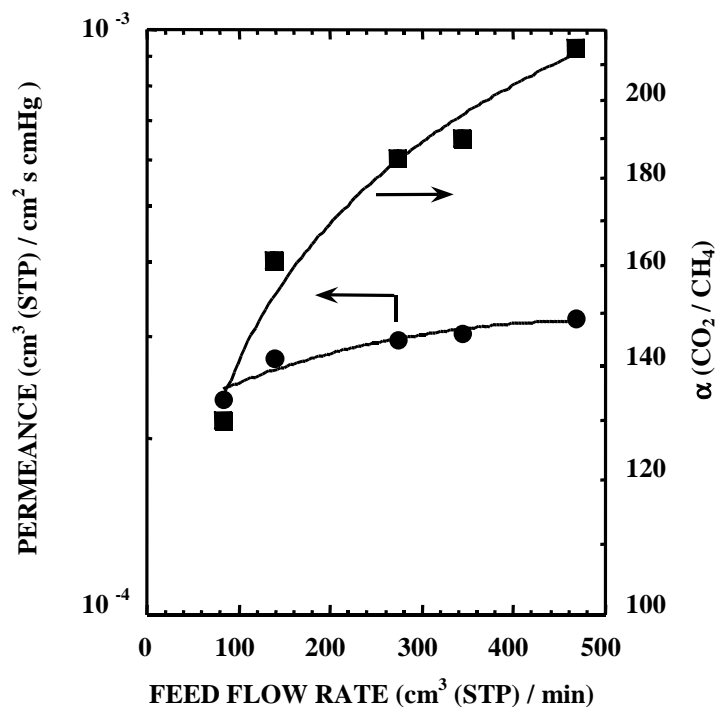


**Figure 3-12**

**CO<sub>2</sub> permeance and CO<sub>2</sub>/CH<sub>4</sub> separation factor versus feed flow rate for separation of a 50/50 (v/v) CO<sub>2</sub>/CH<sub>4</sub> gas mixture. (T = 26 °C, ΔP = 5.5 bar).**

For the investigation of the effect of temperature, experiments were conducted at a constant feed flow rate (stage cut = 9 %) while maintaining a constant pressure gradient across the membrane (ΔP=5.5 bar). The steady-state values of CO<sub>2</sub> permeance and separation factor, α(CO<sub>2</sub>/CH<sub>4</sub>), were assured by reversible heating and cooling. Figure 3-13 shows that the CO<sub>2</sub> permeance increases slightly with temperature while the CO<sub>2</sub>/CH<sub>4</sub> selectivity decreases with temperature. The slight increase in the CO<sub>2</sub> permeance with temperature suggested that in the presence of CH<sub>4</sub>, CO<sub>2</sub> transport is slightly activated by temperature. The drastic decrease in α(CO<sub>2</sub>/CH<sub>4</sub>) at higher temperature was similar to what was observed for pure-gas permeation (Figure 3-7). Moreover, at lower temperature, the mixed-gas α(CO<sub>2</sub>/CH<sub>4</sub>) at high feed flow rates was always higher than the ideal selectivity of pure-gas α<sub>1</sub>(CO<sub>2</sub>/CH<sub>4</sub>). This is due to preferential adsorption of CO<sub>2</sub> inside the pores under mixed-gas feed conditions, which hinders CH<sub>4</sub> transport through the membranes. Comparing Figure 3-7 with Figure 3-13, the difference between α(CO<sub>2</sub>/CH<sub>4</sub>) and α<sub>1</sub>(CO<sub>2</sub>/CH<sub>4</sub>) vanishes at higher temperatures due to the decrease in CO<sub>2</sub> adsorption with increasing temperature.

For investigation of the effect of pressure, the retentate pressure was varied while the temperature ( $T=26^\circ\text{C}$ ) and the permeate pressure (ambient pressure) were maintained constant. Figure 3-14 shows that, under constant feed flow rate and temperature conditions, the  $\alpha(\text{CO}_2/\text{CH}_4)$  is essentially independent of the pressure gradient while the  $\text{CO}_2$  permeance slightly increases with pressure gradient and then levels off at higher pressure gradients. The initial increase in  $\text{CO}_2$  permeance might be indicative of a low  $\text{CO}_2$  coverage on the pore walls at a low-pressure gradient. At higher pressure, once the pore walls were covered with  $\text{CO}_2$ , transport was independent of the pressure gradient.

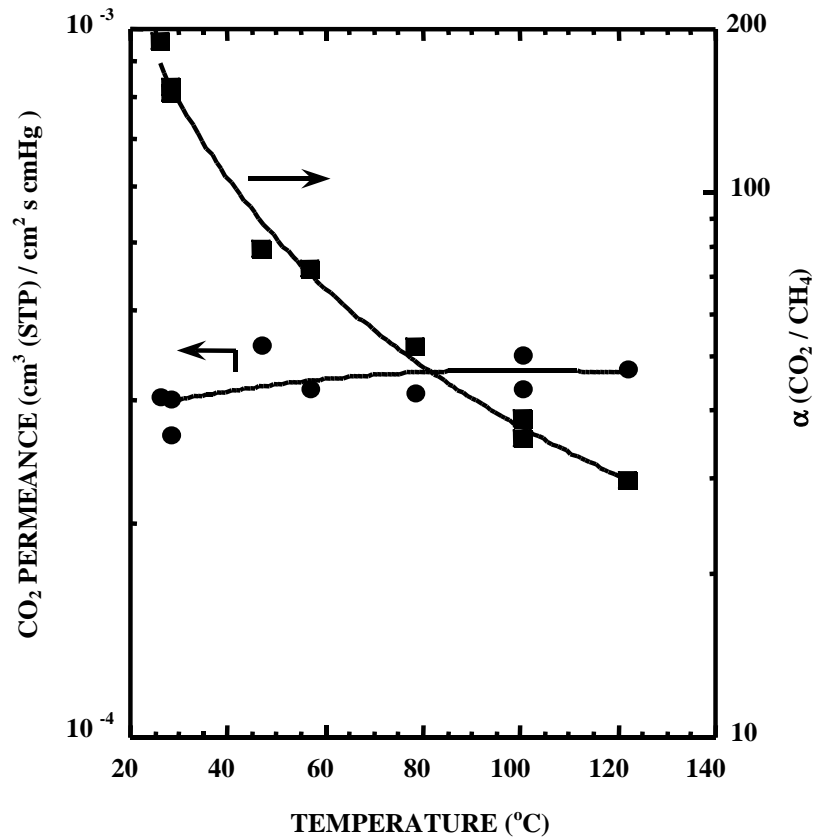


**Figure 3-13**  
 $\text{CO}_2$  permeance and  $\text{CO}_2/\text{CH}_4$  separation factor  $\alpha$  as a function of temperature for separation of a 50/50 (v/v)  $\text{CO}_2/\text{CH}_4$  gas mixture. (Stage cut =9 %,  $\Delta P = 5.5$  bar).

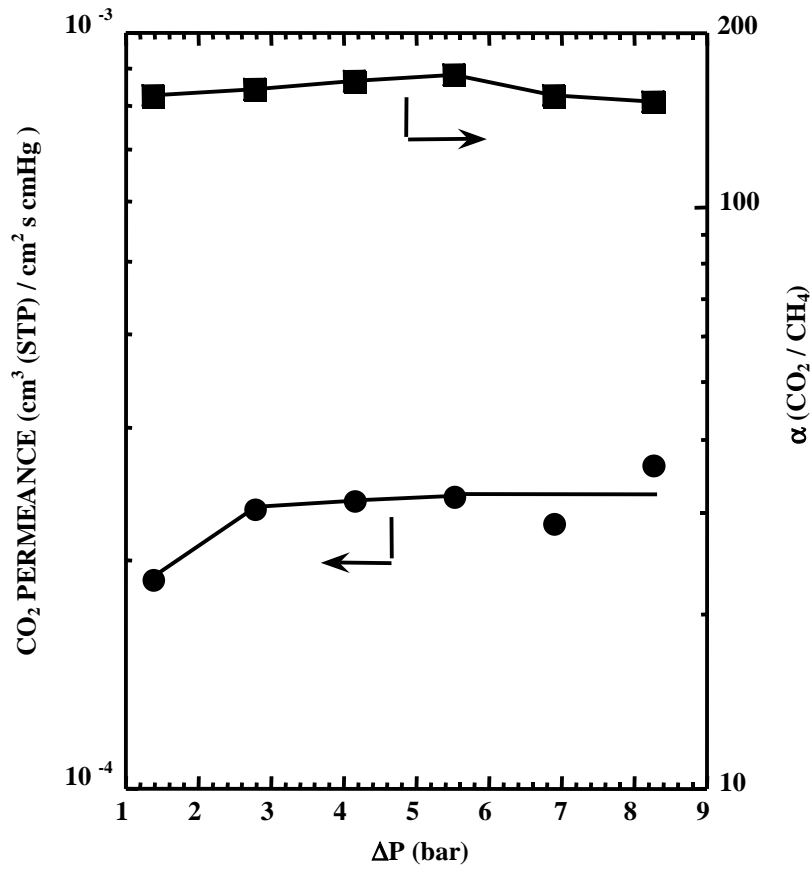


**Figure 3-14**  
 **$\text{CO}_2$  permeance and  $\text{CO}_2/\text{CH}_4$  separation factor  $\alpha$  as a function of pressure gradient for separation of a 50/50 (v/v)  $\text{CO}_2/\text{CH}_4$  gas mixture. (stage cut = 9 %,  $T = 26^\circ\text{C}$ ).**

### 3.6 Hydrogen Purification and NO<sub>x</sub> Removal

The dual-layer silica membrane processed at 300°C was excellent for CO<sub>2</sub>/CH<sub>4</sub> separation but was unable to achieve outstanding H<sub>2</sub> separation due to its relatively large pore size. Pore size could be further reduced via an extended calcination step at 450°C for 1 h in air. Pure-gas permeation at 80°C for the 450°C-calcined membrane is shown in Figure 3-15. Due to the extended calcination, the pore size of the membrane was further reduced, resulting in a sharp molecular-size cut-off near 3.5 Å. With an excellent hydrogen separation factor (H<sub>2</sub>/CH<sub>4</sub>=1265) as well as a high hydrogen permeance ( $1 \times 10^{-3}$  cm<sup>3</sup>(STP)/cm<sup>2</sup>-s-cmHg), such a membrane provides a great opportunity in applications such as hydrogen recovery from petrochemical plants and hydrogen purification for fuel cells. Of relevance to fuel cells, the membrane selectively separated hydrogen from a simulated reformat gas mixture that would result from the partial oxidation of methanol (33.98% N<sub>2</sub>, 15.00% CO<sub>2</sub>, 0.997% CO, balance H<sub>2</sub>). A 92 mole% H<sub>2</sub> purity could be

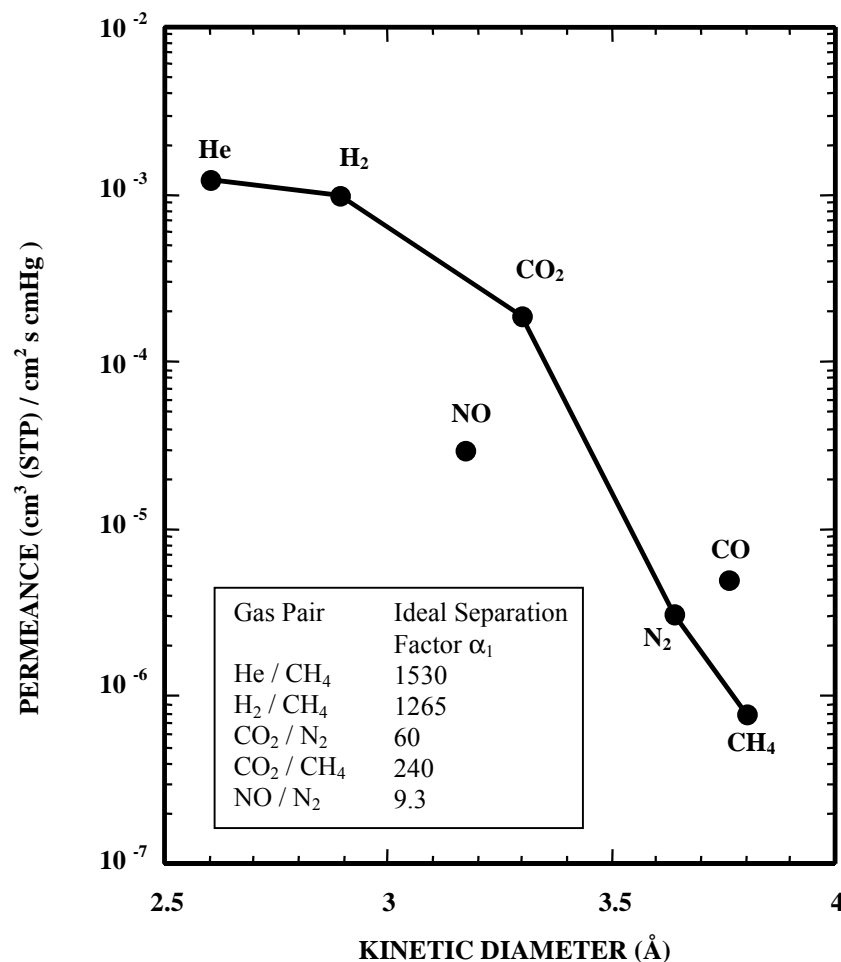


**Figure 3-15**  
Molecular-sieving behavior of a membrane calcined at 450 °C. The ideal separation factor  $\alpha_1$  represents the ratio of permeance (measured in single-gas permeation tests) for two specified gases.

obtained in the permeate stream at a stage-cut of 8.2% (Table 3-2). The CO concentration (CO is a known PEM fuel cell poison) in the permeate stream was reduced to at least fifty times lower than that in the feed. We also achieved a high H<sub>2</sub> permeance ( $6 \times 10^{-4}$  cm<sup>3</sup>(STP)/cm<sup>2</sup>-s-cmHg) and a high H<sub>2</sub>/N<sub>2</sub> separation factor of over 270 for separation of a 50/50 (v/v) H<sub>2</sub>/N<sub>2</sub> gas mixture (Table 3-3). Beside H<sub>2</sub> purification, the membrane could also be used in NO<sub>x</sub> removal from power-plant flue gas. NO/N<sub>2</sub> selectivity and NO permeance reached 9.3 and  $3 \times 10^{-5}$  cm<sup>3</sup>(STP)/cm<sup>2</sup>-s-cmHg, respectively, for pure-gas permeation (Figure 3-15).

**Table 3-2**

**Dual layer membrane calcined at 450 °C for separation of a simulated reformat gas mixture (33.98% N<sub>2</sub>, 15.00% CO<sub>2</sub>, 0.997% CO, and 50.023% H<sub>2</sub>) at 80 °C.**

Gas i	Permeance x 10 <sup>6</sup> cm <sup>3</sup> (STP)/(cm <sup>2</sup> s cmHg)	Separation Factor (H <sub>2</sub> / Gas i)	Single gas permeance ratio	Permeate (mole %)	Retentate (mole %)
H <sub>2</sub>	507	--	--	92.19	43.25
CO <sub>2</sub>	101	5.0	5.2	7.36	16.89
N <sub>2</sub>	2.15	235.9	316.0	0.37	40.47
CO	3.83	132.2	198.6	0.0193	1.14

**Table 3-3**

**Dual layer membrane calcined at 450 °C for separation of a 50/50 (v/v) H<sub>2</sub>/N<sub>2</sub> gas mixture at 80 °C.**

Gas i	Permeance x 10 <sup>6</sup> cm <sup>3</sup> (STP)/(cm <sup>2</sup> s cmHg)	Separation Factor (H <sub>2</sub> / Gas i)	Single gas permeance ratio	Permeate (mole %)	Retentate (mole %)
H <sub>2</sub>	606	--	--	99.41	37.43
N <sub>2</sub>	2.21	274.5	316.0	0.59	62.57

# 4

## REPRODUCIBILITY AND LONG-TERM STABILITY

---

### 4.1 Effect of Environment During Membrane Formation

Commercialization of membrane technology can be influenced by a variety of crucial factors. Beside the desired high selectivity and high permeance, one of the most important factors in membrane technology is easy and cheap membrane processing. The membrane preparation is the first step in the long way of commercializing this technology. In this chapter therefore we investigated the single deposition steps of membrane formation to find the cheapest and easiest way to achieve the previously reported combined high selectivity and permeance. The membrane formation itself by the dip-coating process is a very simple step and does not need any improvements. The membranes reported so far are dip-coated under class-10 environment. This was a point where further attention was drawn. In the following we report of our investigations of how important class-10 clean room conditions really are. Further point of interest was the effect of the quality of the sub-layer, which means the effect of the surfactant used for the preparation of the sub-layer.

To investigate the effect of the environment on membrane deposition, various membranes were prepared using the same sol (same surfactant), but dip-coating in a) a dry nitrogen glove box or b) under class-10 clean room conditions. The dry nitrogen box is a glove box that is constantly flushed with pre-dried nitrogen. The nitrogen gas is not filtered and the humidity in this box varies between 3-6 %. The class-10 clean room box instead is operated by using regular air that is filtered through a 0.3  $\mu\text{m}$  filter. By circulating the air, i.e. reusing the pre-filtered air, the amount of particles of size larger than 0.3  $\mu\text{m}$  that have to be removed is reduced. The amount and size distribution of particles was measured with a laser-based particle analyzer and was proven in each deposition as class-10, which means less than 10 particles of sizes smaller than 0.5  $\mu\text{m}$  per cubic feet of air, averaged over a measuring time of 1 minute. The air stream flows downwards whereas the substrate is withdrawn upwards during dip-coating. As previously shown, the surfactants used in this study are not very sensitive to humidity, so the difference in atmospheric humidity (3-6 % in dry nitrogen box versus ambient 10-30 % in the clean room box) does not seem to affect the structure formed and therefore the properties of the mesoporous silica sub-layers.

Figure 4-1 and Table 4-1 summarize the results of single-gas permeation of membranes deposited in the dry nitrogen box. As clearly seen, membrane deposition in the dry nitrogen box is not very reproducible. The connected black symbols correspond to the best results reported before in chapter 3 and were used as a standard for comparison. All the membranes shown are dual-layer membranes prepared with a  $\text{C}_6$ -templated silica sub-layer. As described before, the surfactant-containing silica sub-layer was vacuum dried for 6 h at 120°C and then calcined in air for 3 h at 450°C. The microporous (solvent-templated) silica layer was calcined for 6 h at 300°C in vacuum.

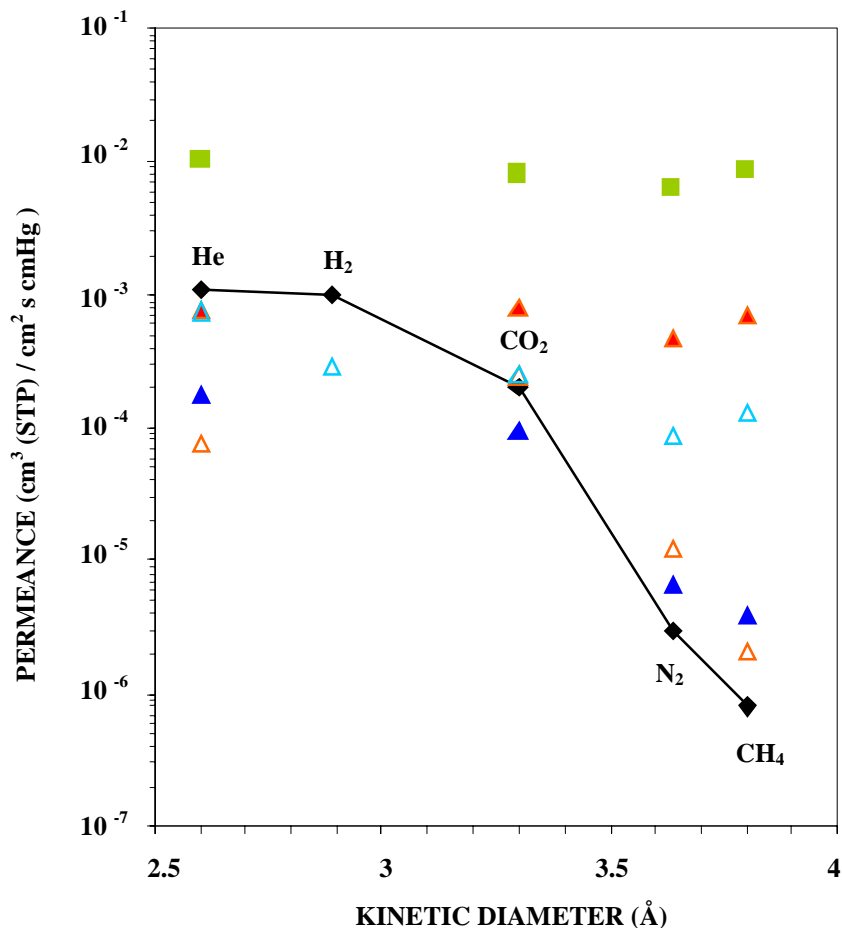


**Figure 4-1**  
 Single gas permeance of membranes deposited in the dry nitrogen box and calcined at 300 °C under vacuum (C<sub>6</sub> was used as template for the silica sub-layer). Triangles correspond to 4 different membranes prepared identically, squares correspond to the permeance of the untreated support, the diamonds corresponds to the best results reported before in chapter 3 and is used as standard for comparison.

**Table 4-1**  
 Ideal selectivity of membranes deposited in the dry nitrogen box (see Figure 4-1).

	He / CO <sub>2</sub>	He / N <sub>2</sub>	He / CH <sub>4</sub>	CO <sub>2</sub> / N <sub>2</sub>	CO <sub>2</sub> / CH <sub>4</sub>	N <sub>2</sub> / CH <sub>4</sub>
Knudsen	3.32	2.65	2.00	0.80	0.60	0.76
untreated support	2.54	2.31	1.87	0.88	0.74	0.79
membrane #1	0.95	1.61	1.10	1.69	1.15	0.68
membrane #2	0.30	6.02	36.98	20.16	123.76	6.14
membrane #3	1.87	26.24	45.10	14.05	24.15	1.72
membrane #4	2.97	8.58	5.94	2.89	2.00	0.69

The variation in gas permeance of these identically prepared membranes is very large. For He and CO<sub>2</sub> gases, the permeances scattered in a range of one order of magnitude. N<sub>2</sub> and CH<sub>4</sub> permeances varied in a range of 3 orders of magnitude. As will be shown below, this large variation in permeance cannot be attributed to the porous tubular support since the variation in the permeances of all measured gases is less than 10 %. Deposition under clean room conditions (Figure 4-2, Table 4-2) instead shows highly reproducible results. The permeances of all four tested membranes are very close to each other, with variation in permeance from one membrane to another of only about 10-20 %. Similar results have been found for the CTAB-templated system as well. Brij-56 seems to follow this trend as well although fewer data points were obtained for this system.

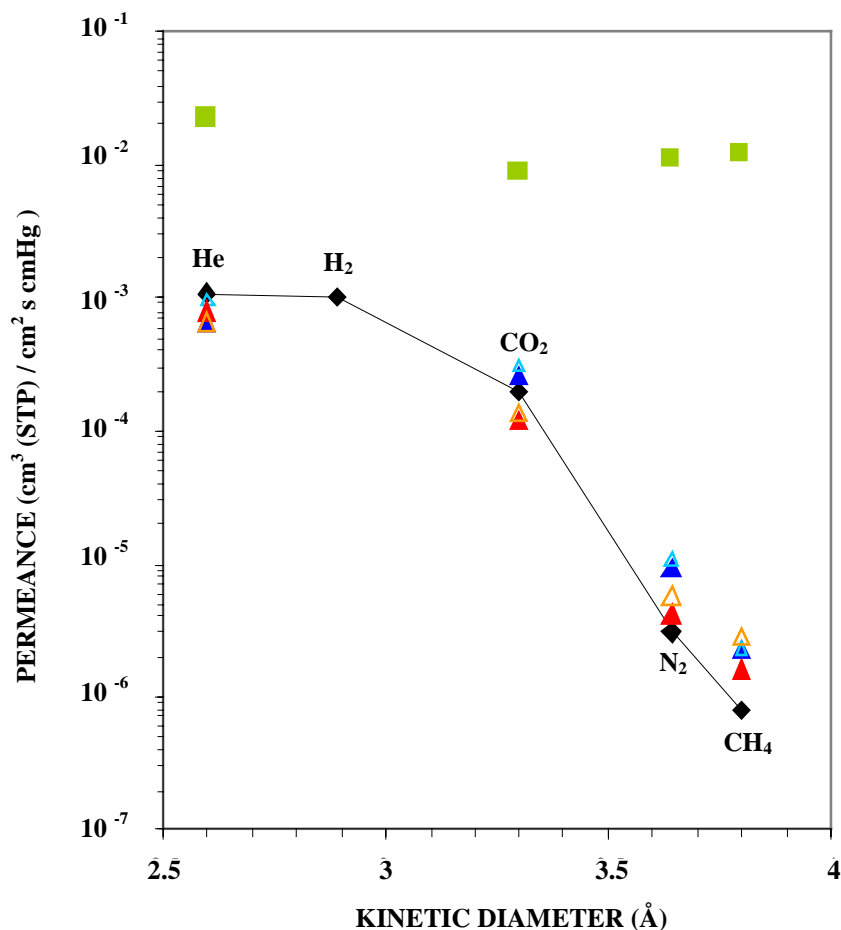


**Figure 4-2**  
 Single gas permeance of membranes deposited under clean room condition and calcined at 300 °C under vacuum (C<sub>6</sub> was used as template for the silica sub-layer). Triangles correspond to 4 different membranes prepared identically, squares correspond to the permeance of the untreated support, the diamonds corresponds to the best results reported before in chapter 3 and is used as standard for comparison.

**Table 4-2**  
**Ideal selectivity of membranes deposited under clean room condition (see Figure 4-2).**

	He / CO <sub>2</sub>	He / N <sub>2</sub>	He / CH <sub>4</sub>	CO <sub>2</sub> / N <sub>2</sub>	CO <sub>2</sub> / CH <sub>4</sub>	N <sub>2</sub> / CH <sub>4</sub>
Knudsen	3.32	2.65	2.00	0.80	0.60	0.76
untreated support	2.54	2.31	1.87	0.88	0.74	0.79
membrane #1	2.48	71.58	285.71	28.85	115.15	3.99
membrane #2	3.20	89.64	428.70	28.00	133.91	4.78
membrane #3	6.51	183.57	485.71	28.17	74.53	2.65
membrane #4	4.75	115.18	229.17	24.26	48.26	1.99

By comparing the membranes deposited under clean room conditions with those formed in the unfiltered environment, it seems that membranes formed in non-filtered air are more susceptible to defect formation, which causes the poor reproducibility in permeation properties. The membranes deposited under class-10 clean room conditions instead contain much fewer defects, and as a result, show both good reproducibility in transport properties as well as high ideal selectivities. These experimental results justify previous concerns on the need of a clean environment for membrane deposition.

Further testing of the deposition in unfiltered atmosphere (dry nitrogen) or clean room condition was done by measuring the permeance of a small gas, such as hydrogen or helium, through membranes which were not calcined prior to the permeation experiment. This testing was carried out on the uncalcined surfactant-templated sub-layer, since the quality of the substrate surface on which the selective top-layer was deposited seemed to be the most crucial factor for good membrane performance. The permeance of the pure untreated 50 Å  $\gamma$ -Al<sub>2</sub>O<sub>3</sub> support (averaged over 3 different tubes) is compared with the He-permeance of uncalcined C<sub>6</sub> surfactant-templated silica layers, deposited in either dry nitrogen box or under class-10 clean room condition (Figure 4-3). Since the silica membrane is not calcined the pores are still filled with the surfactant molecules. Assuming a continuous and defect free coating, no or very little permeance is expected. The untreated support has a permeance of about 10<sup>-2</sup> cm<sup>3</sup>(STP)/cm<sup>2</sup>-s-cmHg for all gases measured. After coating a C<sub>6</sub>-templated silica sub-layer over the support tube in the dry nitrogen condition, the H<sub>2</sub>-permeance drops 3 orders of magnitude, indicating good coverage of the 50 Å  $\gamma$ -Al<sub>2</sub>O<sub>3</sub> support. However, the membrane formed using the same sol (C<sub>6</sub>), but dip-coated under clean room condition shows even one order of magnitude lower permeance for He, proving that class 10-clean room condition leads to membranes with much smaller number of defects. Furthermore, it was observed that CTAB-templated sub-layers lead to a He permeance which is 2-3 times lower than that of respective C<sub>6</sub> coatings. This indicates that CTAB-templated sub-layers achieve better coverage or contain fewer defects compared to respective C<sub>6</sub>-sublayers.

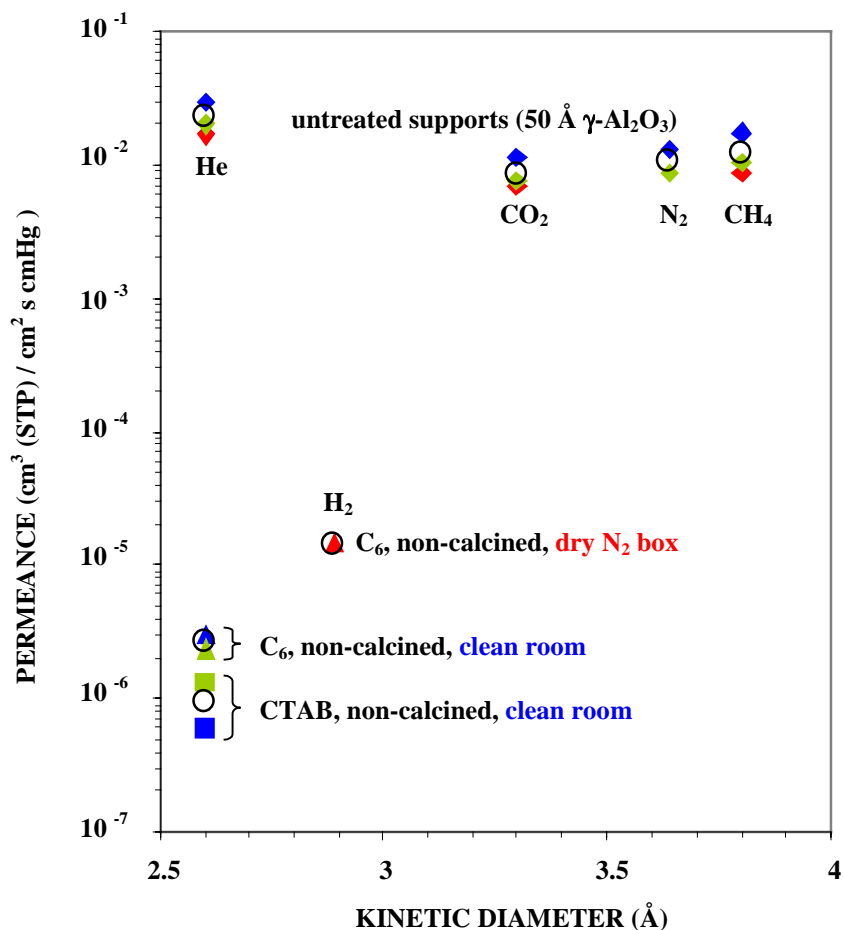


**Figure 4-3**  
Comparison of the coating environment: dry nitrogen box (unfiltered Atmosphere) versus class-10 clean room condition.

## 4.2 Effect of Calcination Conditions

The final goal of this work is the development of highly selective membranes for separation processes such as natural gas purification, NO<sub>x</sub> removal or CO<sub>2</sub>/CH<sub>4</sub> separation. All these separations are pressure-based separations and the gas mixtures can contain a certain amount of water. To maintain a good membrane performance either the membrane needs to be stable to high humidity or the feed stream needs to be dried prior its contact with the membrane. Although a pre-drying step would increase the operating costs of a membrane separation process, it might be justifiable if the membrane shows much better performance with pre-dried feeds. The membranes discussed so far were calcined in vacuum with the intention to form a carbon coating on the pore surface and to change the surface chemistry from highly hydrophilic to highly hydrophobic. The carbon coating formed by vacuum calcination and the accompanied hydrophobicity of the membrane surface protect the membrane from water attack. In this way a pre-drying step would not be necessary. Nevertheless, it is worth to investigate if the membrane performance can be improved orders of magnitude if the calcination is done differently, such as

in different atmosphere (air instead of vacuum) or at different temperatures. Figure 4-4 shows a comparison between vacuum and air calcination of dual-layer membranes (calcined at 300°C), with a C<sub>6</sub>-templated sub-layer. The membranes were coated under clean room condition, which leads to reproducible results. All data points are averaged over 3 single measurements with an error bar of about 15%. No significant difference has been observed between calcination in air or in vacuum. Both calcination conditions seem to result in the same membrane performance. Therefore, vacuum calcination is preferable during membrane processing since the carbon coating formed by this way will provide a protective layer for water attack and may therefore increase the membrane life-time. However, it still needs to be confirmed experimentally whether the membrane can retain its high permeance and selectivity after prolonged contact with humidified feeds.

The variation of the calcination temperature from 300°C to 450°C did not lead to consistent results. Some membranes showed the same performance with the membranes calcined at 300°C discussed before, but others seemed to crack by the higher temperature treatment. In these cases a very high permeance for all gases was observed with a selectivity comparable to Knudsen selectivity.

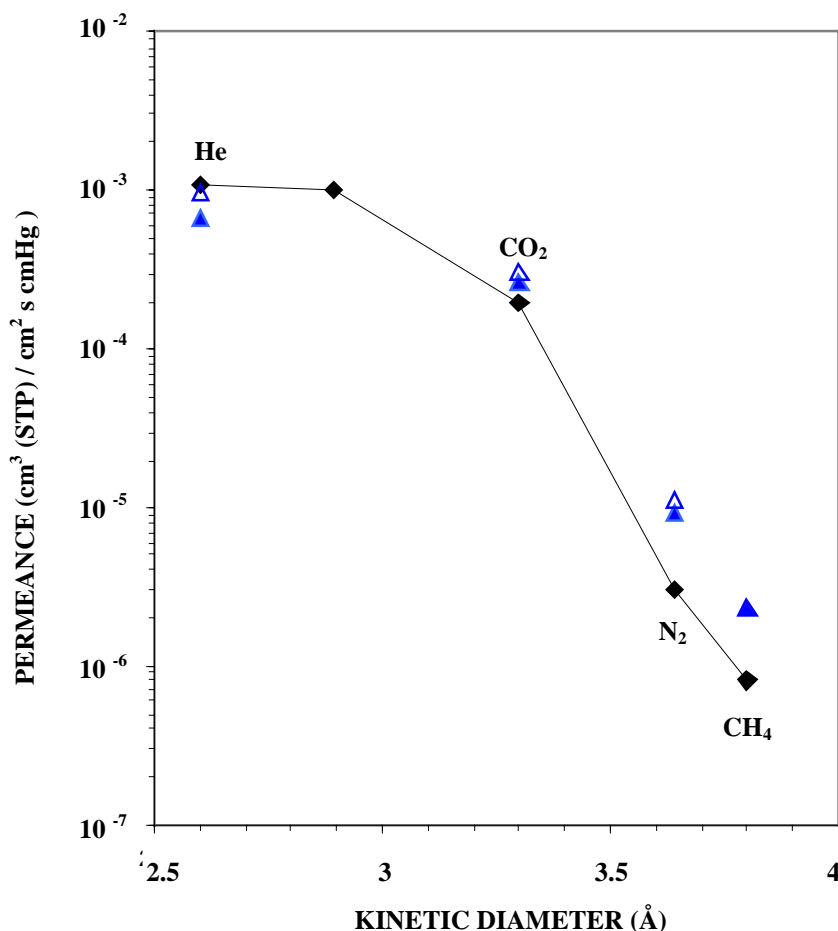


**Figure 4-4**  
Comparison of the calcination condition: vacuum versus air.

### 4.3 Long-term Stability

A dual-layer membrane consisting of a C<sub>6</sub>-templated silica sub-layer and vacuum calcined at 300°C was operated for 150 h under constant temperature, pressure gradient, and feed flow rate conditions (Figure 4-5). Due to the gradual removal of pre-adsorbed moisture during this extended permeation test, both the CO<sub>2</sub> permeance and  $\alpha(\text{CO}_2/\text{CH}_4)$  gradually increased with time. To avoid any pre-adsorbed moisture, a freshly-prepared membrane was evacuated at 80°C inside the permeation cell for 3 h prior to the permeation experiments. The membrane was then pressurized with a sequence of pure gases until steady state was reached. Depending on the gas and temperature, steady state needed between 4 and 16 h. Figure 4-6 gives the summary of this experiment with the steady state values for each single gas and each temperature. The numbers give a guideline on the sequence of gases and temperature measured. For all gases, the permeances at 80°C are higher compared to the room temperature values. This is due to a decreased activation barrier at elevated temperature. Prior to the whole experiment and after measuring gases such as CO<sub>2</sub> or CH<sub>4</sub>, the membrane was outgassed, e.g. heated in

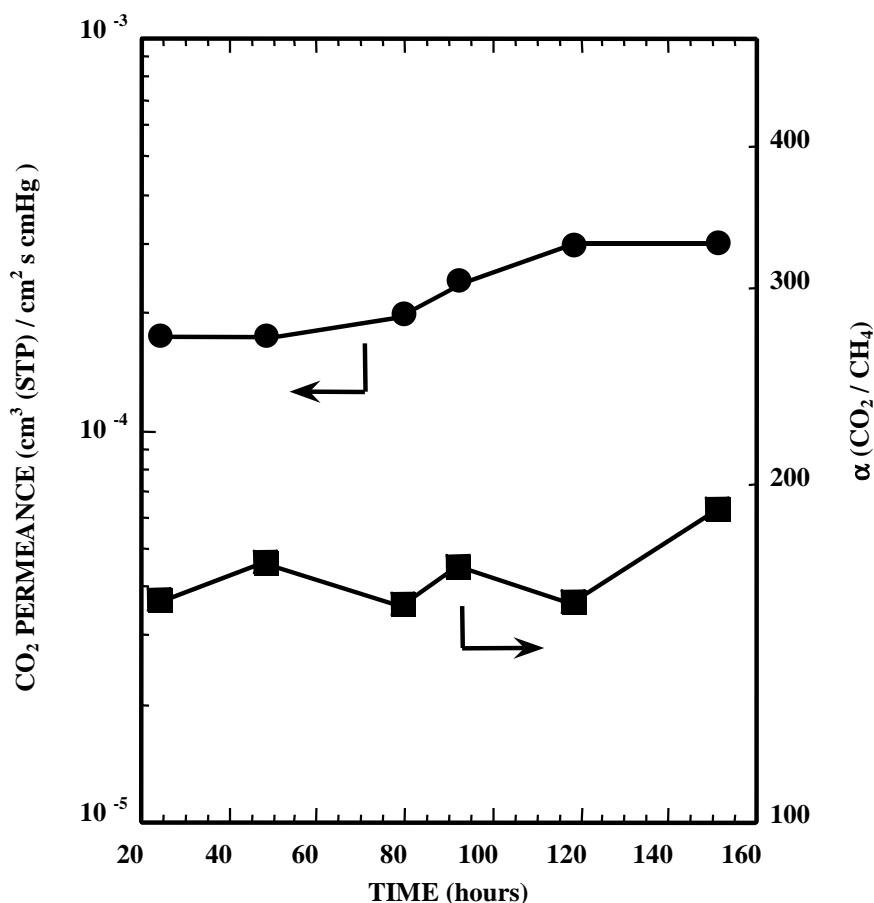


**Figure 4-5**  
C<sub>6</sub>-templated dual layer membrane (calcined at 300 °C under vacuum) continuously operated for 150 hours under conditions of constant temperature (T = 26 °C), pressure gradient ( $\Delta P = 5.5$  bar), and feed flow rate (345 SCCM).

vacuum at 80°C to remove all residues of the previous gas measured and to make sure that accurate permeances are obtained for the following gas. The entire experiment with switching gases, outgasing between gases and measuring at different temperatures lasted over a period of more than 2 weeks. In this time the membrane was heated for about 1 week continuously at 80°C, plus additional eight times for about 4 h each during the outgasing step. At the end of this experiment the He permeance was measured again to determine whether the performance of the membrane has changed during this long operating time. As can be seen in Figure 4-6, by comparing He permeance # 1, which was measured right at the beginning of the experiment, with He permeance # 9, which was measured as well at room temperature but after the long pressure and temperature treatment, no significant change of the membrane performance has occurred.

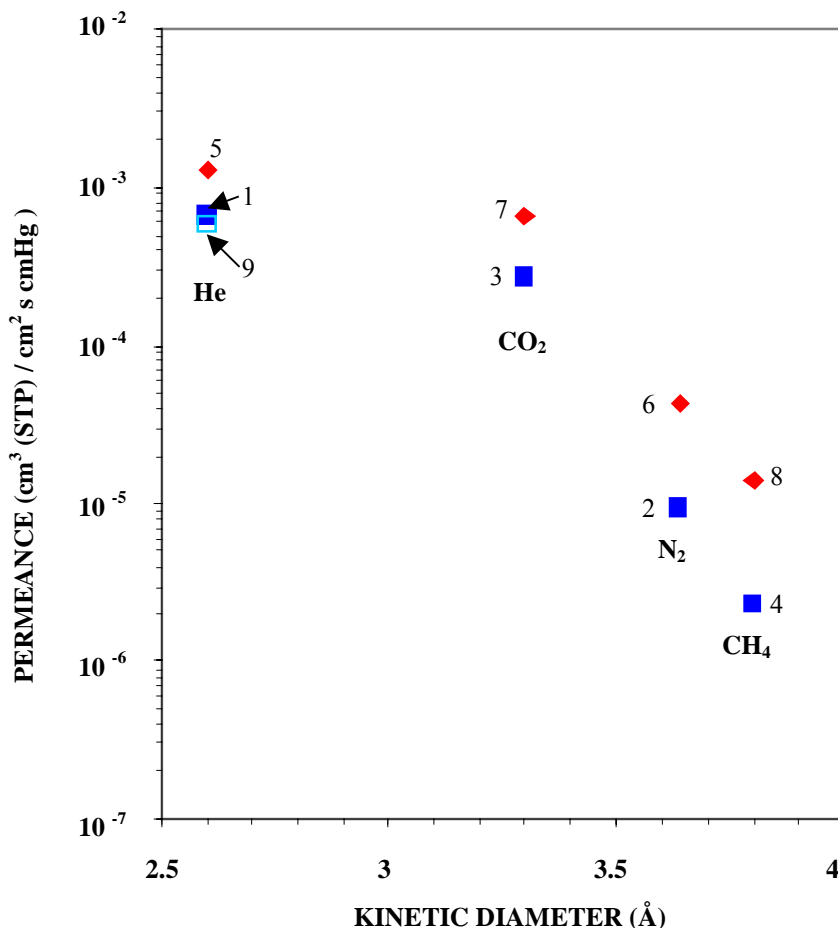


**Figure 4-6**  
**Long-term stability of a dual layer membrane. Total time of the experiment was 2 weeks.**  
**The numbers correspond to the sequence of permeation measurements. Squares**  
**corresponds to room temperature, diamonds to 80 °C.**

## 4.4 Overview of Membrane Formation

Summarizing all the above with regard to the formation of dual-layer silica membranes, it could be shown that by deposition of: 1) a surfactant-templated silica sub-layer and – after vacuum drying and calcination – 2) a water/ethanol solvent-templated silica top-layer, highly selective membranes can be formed. Compared to our previous results on dip-coating two identical solvent-templated silica layers onto porous ceramic supports, the approach of two asymmetric silica layers used in this work leads to higher permeance as well as higher selectivity. The high selectivity can be explained by a reduction in the amount of defects by: 1) dip-coating under class-10 clean room conditions and 2) by better coating on the surfactant-templated silica sub-layer. The increased permeance instead is the result of the smoother support surface after it has been coated with the surfactant-templated sub-layer leading to a much thinner selective top-layer. The mesoporous silica sub-layer therefore has two effects, it smoothens the surface of the underlying support and it gradually reduces the pore size, thus the solvent-templated silica top-layer does not penetrate inside the underlying silica sub-layer or support. In contrary to double coating of microporous solvent-templated silica layers, as reported in our last report [1], the mesoporous surfactant-templated silica sub-layer (after calcination) does not affect the permeability of the supporting ceramic tube.

The development of these highly selective membranes is summarized in Figure 4-7 on the example of a C<sub>6</sub>-templated dual-layer silica membrane. Initially the permeance of all gases through the untreated 50 Å  $\gamma$ -Al<sub>2</sub>O<sub>3</sub> substrate is of the order of 10<sup>-2</sup> cm<sup>3</sup>(STP)/cm<sup>2</sup>-s-cmHg (circles in Figure 4-7). After dip-coating the surfactant-templated silica sub-layer, the permeance drops about 5 orders of magnitude prior to calcination, since its pores are still filled with the surfactant (triangle in Figure 4-7). Despite minor differences in the quality of the support coverage between the surfactants used (as discussed before in chapter 4.1) this could be observed for all 3 surfactants used in this study, namely C<sub>6</sub> (hexyltriethylammonium bromide), CTAB (cetyltrimethylammonium bromide) and Brij-56. After calcination of the surfactant-templated silica sub-layer, the permeance of all gases is restored again and reaches the same level as the untreated ceramic support (squares in Figure 4-7). Dip-coating and suitable calcination of the microporous silica top-layer finally leads to the highly selective and highly permeable membranes discussed before in detail. No difference has been observed between vacuum and air calcination.

This approach is generally applicable for a variety of surfactant-templated silica layers that can be used as sub-layers to smoothen the rough support surface and to gradually decrease the pore size. Thus, the second selective layer can be deposited as a thin and defect-free membrane. Generally the selective top-layer can be formed by various solvent-templated silica sols (as discussed previously [1]) or by various molecular-templated sols, depending on the pore size required for the targeted separation.

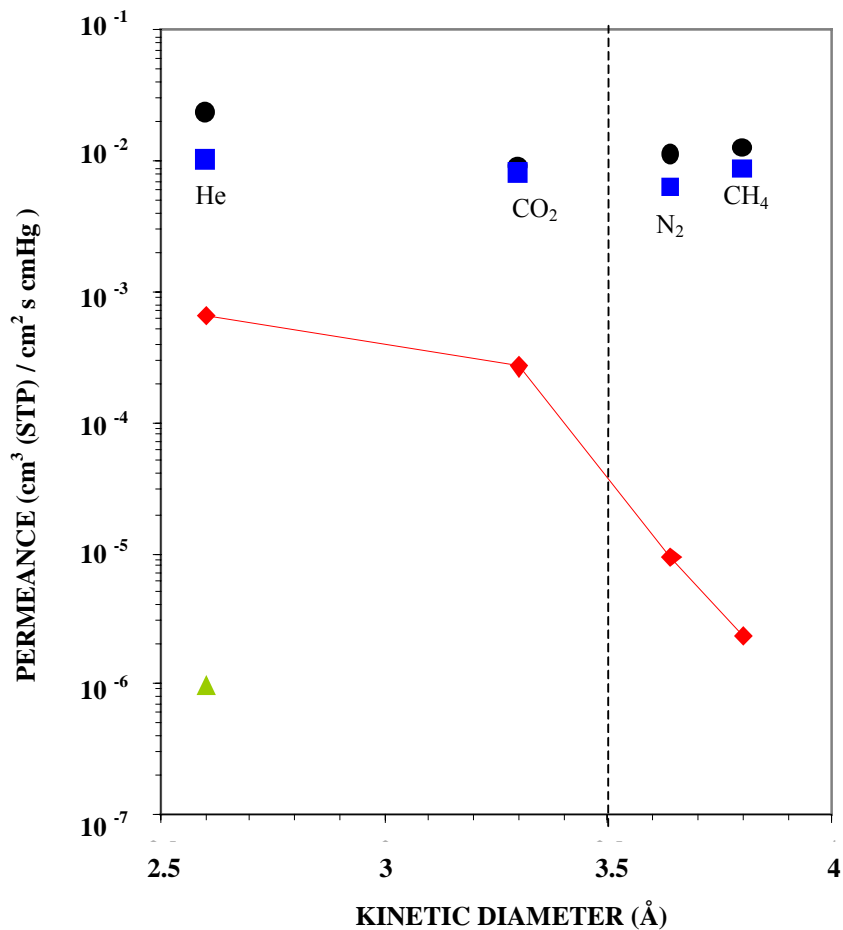


**Figure 4-7**  
 Step-by-step development of highly selective silica dual layer membranes. Circles corresponds to the untreated  $50 \text{ \AA}$   $\gamma$ -alumina support, triangles to the non-calcined surfactant templated silica sub-layer, squares to the calcined surfactant templated silica sub-layer and diamonds to the microporous selective silica top-layer.

# 5

## USE OF LARGER PORE SIZE SUPPORTS

---

Beside a high selectivity, the main criterion of good membrane performance is a high permeation rate through the membrane. Since the inorganic membranes reported here are supported membranes, the relative pore size and thickness of the support tube may significantly contribute to the flow resistance through the entire membrane system. All work reported so far here was carried out using 50 Å  $\gamma$ -Al<sub>2</sub>O<sub>3</sub> supports. These are the smallest pore size ceramic supports commercially available. To increase the permeance while keeping the same high selectivity, one approach is to change the support material to a coarser one. Since it has not been tested yet if continuous membranes can be formed over 100, 200, 2000 Å or even higher pore size supports, we will report in this chapter on our experiments of membrane formation on such large-pore supports which may be more advantageous with regard to cost as well as permeation resistance reduction.

### 5.1 Deposition by Dip-coating

Three different commercial ceramic tubular supports were employed and three different surfactants were used for templating the silica sub-layer. As described before, the quality of the coating was determined by measuring its permeance prior to calcination. Since the pores are still filled with the surfactant molecules, no or very little permeance is expected in case of a continuous and defect-free coating. The ceramic tubes chosen for this study were a 50 Å  $\gamma$ -Al<sub>2</sub>O<sub>3</sub> support (coarse  $\alpha$ -Al<sub>2</sub>O<sub>3</sub> coated on the inner surface with 50 Å  $\gamma$ -Al<sub>2</sub>O<sub>3</sub>), a 200 Å  $\gamma$ -Al<sub>2</sub>O<sub>3</sub> support (coarse  $\alpha$ -Al<sub>2</sub>O<sub>3</sub> coated on the inner surface with 200 Å  $\gamma$ -Al<sub>2</sub>O<sub>3</sub>) and a plain  $\alpha$ -Al<sub>2</sub>O<sub>3</sub> support of 0.2  $\mu$ m pore size. Surfactants used were C<sub>6</sub>, CTAB and Brij-56. All membranes were dip-coated under class-10 clean room condition and predried at 120°C under vacuum, but not calcined. As shown in [Figure 4-3](#) very good coverage can be achieved on the 50 Å  $\gamma$ -Al<sub>2</sub>O<sub>3</sub> supports. The permeance of the uncalcined surfactant containing silica sub-layer is of the order of 10<sup>-6</sup> cm<sup>3</sup>(STP)/cm<sup>2</sup>-s-cmHg. As already mentioned before, it has been observed that CTAB-templated silica sols seem to better cover over the rough surface of the ceramic support. Their permeance is about 2-3 times lower than the uncalcined C<sub>6</sub>-templated sub-layers.

Using a 2000 Å ceramic tube, some flow resistance was added by the uncalcined mesoporous sub-layer as can be seen by the decrease in the permeance of all gases ([Figure 5-1](#)) but the coverage was not perfectly continuous. The permeance is lowered only by about 1 to 1.5 orders of magnitude, which indicates a high amount of defects, cracks or more probably pinholes. The pores of the underlying support seem to be too large to be covered by the sol during the dip-coating process. Future experiments are planned in order to test if a second dip-coating using the same surfactant containing sol can heal the defects observed in the first coating. But nevertheless, as observed before on 50 Å  $\gamma$ -Al<sub>2</sub>O<sub>3</sub> supports, CTAB shows better coverage than

C<sub>6</sub>-surfactant. Brij-56 was tested a single time and showed similar results as CTAB. Possible improvements planned for future work on this point is the use of aged surfactant-containing sols. Aging should lead to larger polymeric units, which will not penetrate into the support but span over the even larger pores. In this way, the formation of continuous membranes even over larger pore size supports should be possible at least up to a certain limit of maximum pore size, which still needs to be determined. Using an intermediate pore size support, the 200 Å  $\gamma$ -Al<sub>2</sub>O<sub>3</sub> support, only preliminary results can be reported, but not reproduced yet.

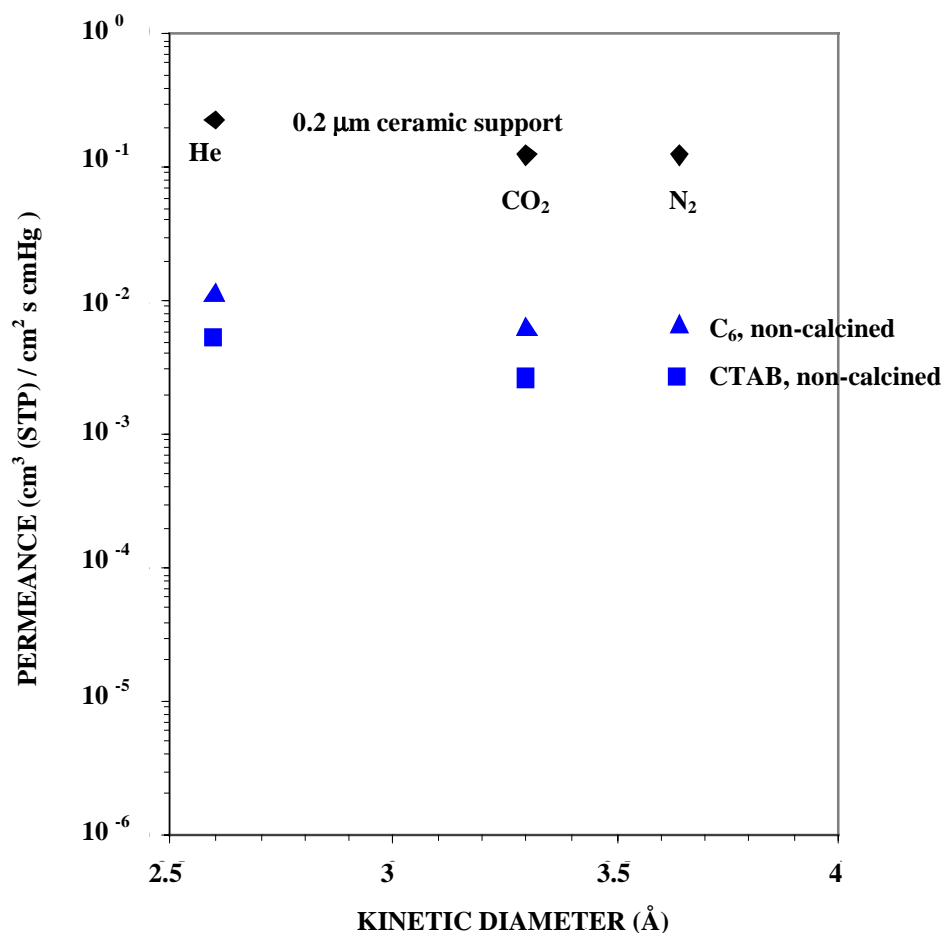


**Figure 5-1**  
**Dip-coating over larger pore supports using the same sol as before**

The commercial 50 Å  $\gamma$ -Al<sub>2</sub>O<sub>3</sub> support is an asymmetric support which consists of a coarse  $\alpha$ -Al<sub>2</sub>O<sub>3</sub> carrier support. This is coated with several layers of  $\gamma$ -Al<sub>2</sub>O<sub>3</sub> with gradually decreasing particle size, and therefore gradually decreasing pore size until the last layer of 50 Å pore size is reached. The difference between this type of asymmetric support and a large pore support coated with a single mesoporous silica layer is the absence of the fine-pore  $\gamma$ -Al<sub>2</sub>O<sub>3</sub> layers which may add flow resistance to the overall support/membrane system. The possibility of coating mesoporous silica sub-layers over large-pore supports therefore has two important advantages: 1) it reduces the cost of the support system, since additional ceramic coatings necessary to

gradually reduce the final pore size are not required anymore and 2) the permeation resistance through the support is reduced by eliminating the small-pore  $\gamma$ - $\text{Al}_2\text{O}_3$  layers. Thus, it is worth further trying to coat continuous mesoporous membranes over large-pore supports for the purpose of utilizing such inexpensive supports while obviating the additional flow resistance of  $\gamma$ - $\text{Al}_2\text{O}_3$  layers previously employed to improve the ‘surface finish’ of the coarse-pore supports.

## 5.2 Deposition by Aerosol Process

The previous discussion suggested that deposition of surfactant-templated silica sub-layers on larger pore supports (e.g.  $0.2\ \mu\text{m}$   $\alpha$ - $\text{Al}_2\text{O}_3$  tubes) by regular dip-coating appeared to be rather unsuccessful, as indicated by the data shown in Figure 5-1. On the other hand, high-quality Brij-56-templated mesoporous silica layers could be formed on home-made,  $0.2\ \mu\text{m}$   $\alpha$ - $\text{Al}_2\text{O}_3$  disks by suspending the mother silica sol in the gas phase and delivering the resulting aerosol to the surface of the substrate disk by a nitrogen carrier stream. The aerosol generation was implemented with the aid of a humidifier which allowed for nebulization of a small column of the silica sol kept inside a vertical pipe with its bottom closed with a plastic cup which acted as a vibrating diaphragm transmitting the pulsation of the humidifier to the sol. Figure 5-2 is a schematic representation of the experimental set-up for aerosol deposition of surfactant-templated silica sols on top of large-pore disk-shaped ceramic supports (diameter 22 mm).

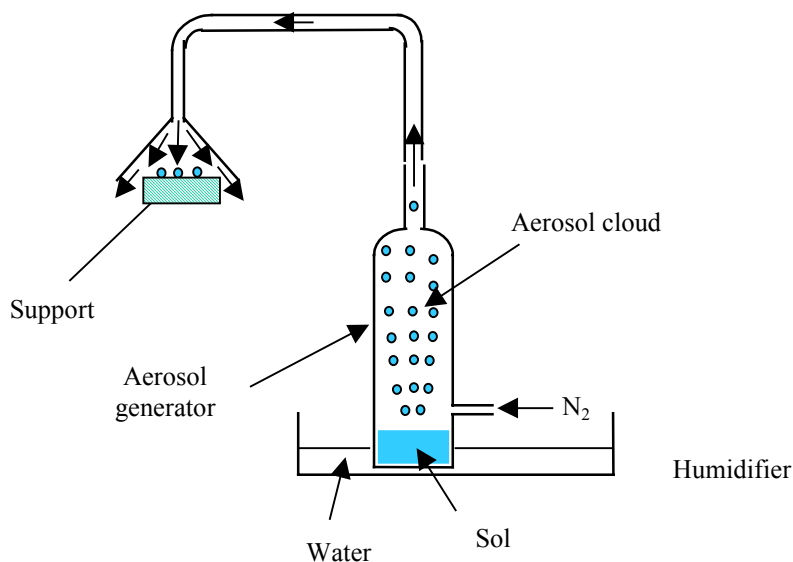


**Figure 5-2**  
Setup for aerosol deposition of surfactant-templated silica sols on planar substrates

At the early stages of aerosol deposition of a surfactant-containing silica sol on a given substrate, liquid droplets deposit from the gas phase on the substrate surface resulting in a monolayer that partially covers the substrate surface. Simultaneously, solvent evaporation results in increase of surfactant concentration in the deposited droplets beyond the critical micelle concentration (cmc) and subsequent onset of self-assembly and formation of mesophases in the partially dried droplets. Continuous arrival of fresh droplets on the substrate surface results in coalescence of

individual droplets of close proximity and finally, after a certain extent of deposition, to a continuous solvent-silica-surfactant film that spans the entire surface of the substrate. Interruption of the deposition process beyond this point and complete evaporation of the solvent may lead to a thin, surfactant-templated mesoporous silica film that, in case of large-pore substrates, can provide a smooth overlayer for subsequent deposition of a microporous silica membrane by regular dip-coating

The quality of the deposited mesoporous silica sub-layers was investigated by N<sub>2</sub> permeation before calcination but after drying overnight at ambient or for 6 h at 120°C in vacuum. The treated disks were sealed with silicon O-rings inside a stainless-steel permeation cell with the coated surface facing the feed side while the opposite side was flushed with a Helium sweep stream with its composition for N<sub>2</sub> analyzed on-line by GC equipped with thermal conductivity detector and a six-port gas sampling valve. After aerosol deposition, the permeance of the support disks decreased several orders of magnitude, suggesting a good coverage of the support surface with mesoporous silica. Specifically, the N<sub>2</sub> permeance decreased from an initial level of  $\sim 10^{-2}$  down to  $10^{-5}$ - $10^{-6}$  cm<sup>3</sup>(STP)/cm<sup>2</sup>-s-cmHg, which is comparable to the gas-tightness achieved by regular dip-coating of the 50 Å  $\gamma$ -Al<sub>2</sub>O<sub>3</sub> substrates (see Figure 4-3). SEM analysis revealed the presence of relatively smooth coatings on top of the supports that completely masked their rough, granular surface. Figure 5-3 shows representative planar views of a ceramic support before (a) and after  $\sim 30$  min aerosol deposition (b), respectively.

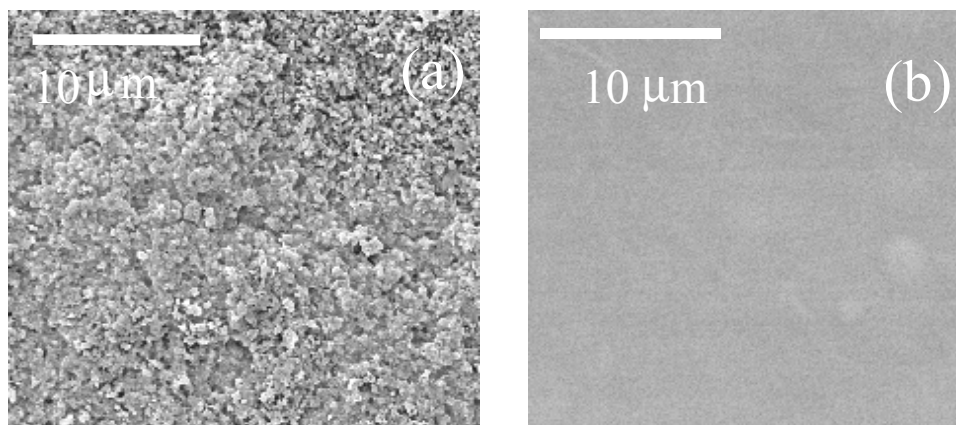


**Figure 5-3**  
**Planar view of a ceramic support before (a) and after (b) aerosol deposition of Brij-56-templated silica sols.**

Future work plan includes the following tasks: (a) attempt to reduce the aerosol deposition time necessary for complete coverage of the support surface down to  $\sim 5$  min. That could be achieved by employing higher N<sub>2</sub> carrier flow rates, or alternatively pull vacuum from the back side of the substrate to enhance aerosol transport to its surface; (b) investigate the gas transport properties and quality of these mesoporous silica sub-layers after calcination for template removal; and ultimately (c) attempt to deposit microporous silica top-layers on top of these aerosol-treated ceramic disks and compare their separation performance with that of tubular membranes made by regular dip-coating.

# 6

## COMPARISON TO LITERATURE

A large number of literature reports are available on membrane-based separations (such as gas permeation, pervaporation, water purification/filtration), primarily dealing with organic polymer membranes. Polymeric membranes may exhibit attractive selectivities for specific gas pairs, but as often observed, there is an inherent trade-off between selectivity and permeance, such as that shown in Figure 6-1 for O<sub>2</sub>/N<sub>2</sub> separation [25]. Polymeric membranes that show very high selectivity usually have very low permeance and vice versa. Due to this trade-off and the low stability of polymer membranes, more and more attention is drawn on inorganic membranes since these are not limited by such a trade-off between permeance and selectivity.

The dual-layer silica membranes we reported above show a very high CO<sub>2</sub> permeance of  $3.2 \times 10^{-4}$  cm<sup>3</sup>(STP)/cm<sup>2</sup>-s-cmHg and a separation factor  $\alpha$  of over 200 for the separation of a 50/50 (v/v) CO<sub>2</sub>/CH<sub>4</sub> gas mixture. This was achieved by operating at room temperature, a moderate pressure gradient of  $\Delta P=5.5$  bar and a high feed flow rate of  $\sim 500$  cm<sup>3</sup> (STP)/min. The dual-layer silica

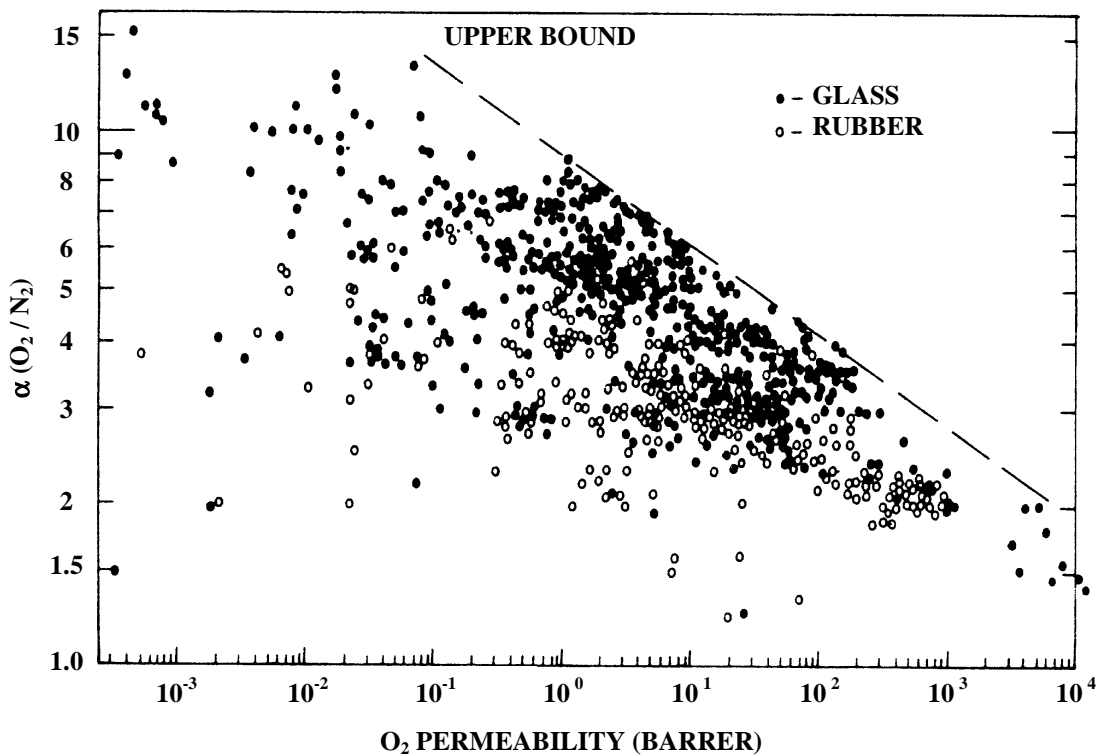


**Figure 6-1**  
Trade-off between selectivity and permeability of polymeric membranes shown at the example of O<sub>2</sub> / N<sub>2</sub> separation [25].

membrane with a C<sub>6</sub>-templated silica sub-layer and calcined at 300°C showed a combination of high permeance and high selectivity. This membrane was superior to gas separation membranes reported so far in the literature [21,26-28]. Dual-layer membranes calcined at 450°C instead have a higher CO<sub>2</sub>/CH<sub>4</sub> separation factor ( $\alpha \sim 600$ ) at the expense of CO<sub>2</sub> permeance (Figure 6-2). Since all membranes made of different materials were all operated under different conditions to achieve their best performance, it is difficult to compare various types of membranes under the same operating conditions. For example, polyimide membranes tend to be operated with a low CO<sub>2</sub>-partial-pressure feed stream to alleviate CO<sub>2</sub> plasticization [27]. Polyelectrolyte membranes based on facilitated transport were also operated with low CO<sub>2</sub>-partial-pressure feed streams to achieve higher CO<sub>2</sub> permeance [26]. Some silica membranes were operated at higher temperatures with sweeping gas [23], while zeolite Y membranes were operated at room temperature to benefit from CO<sub>2</sub> selective adsorption [28]. However, our dual-layer membranes still show superior performance when compared to other literature membranes operated at their optimum conditions.

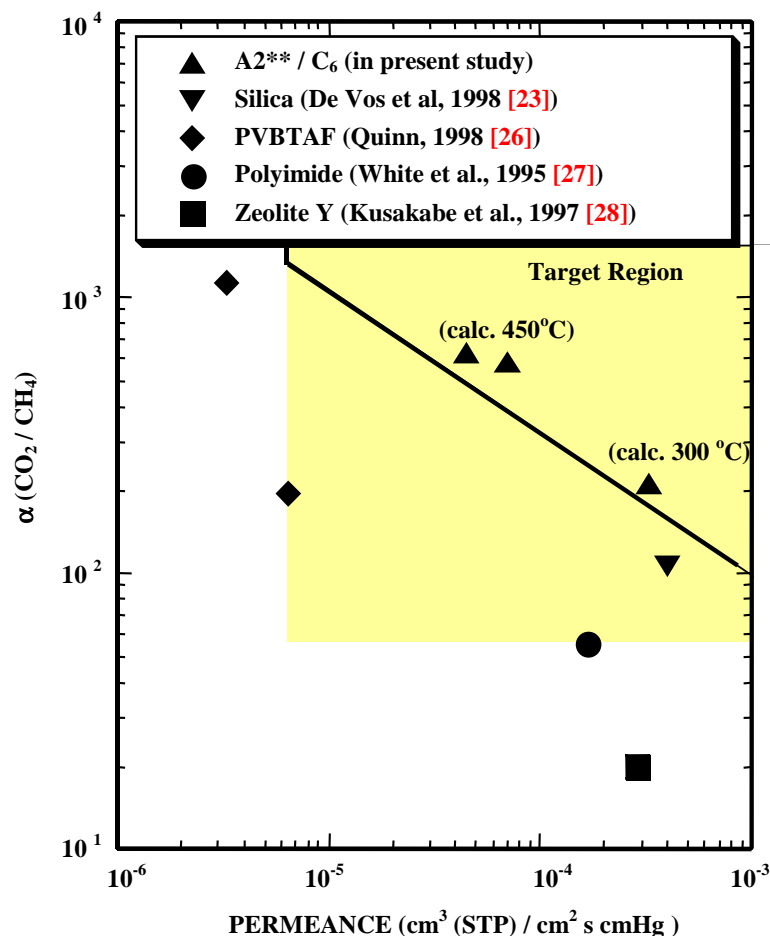


Figure 6-2

Comparison of reported membranes for a mixed-gas, CO<sub>2</sub>/CH<sub>4</sub> separation, (a) present A2\*\*/C<sub>6</sub> membrane, vacuum calcined at 300 °C or 450 °C, (b) silica membrane [23] (CO<sub>2</sub> permeance at 100 °C estimated from reported single-component permeation), (c) polyelectrolyte (PVBTAF) membrane [26], (d) polyimide membrane [27], and (e) Zeolite Y membrane [28].

# 7

## CONCLUSIONS

---

With our new approach of dual-layer silica membranes, both permeance and selectivity could be improved simultaneously. The quality of the support is crucial for the quality of the overlying membrane layer. Pinholes and surface roughness on the support normally produce defects in the subsequently deposited membrane. By depositing first a surfactant-templated micro- or mesoporous intermediate layer on top of a commercial  $\gamma$ -Al<sub>2</sub>O<sub>3</sub> support, it is possible to improve the surface finish of the support and prevent the subsequently deposited sol from penetrating deep into its pores. Three different surfactants have been tested, (hexyltriethylammonium bromide, C<sub>6</sub>), (cetyltrimethyl-ammonium bromide, CTAB) and Brij-56. Furthermore, membranes were dip-coated under class-10 clean room conditions to avoid dust contamination and were vacuum-calcined at 300°C for 6 h to promote further pore shrinkage. The vacuum calcination procedure apparently also resulted in the decomposition of surface ethoxy groups; therefore, a more hydrophobic pore surface was formed as evidenced by an increase in the water contact angle. Calcination in air resulted in the same membrane performance. No difference has been observed in either permeance or selectivity. The dual-layer approach enhanced both flux and selectivity of an asymmetric membrane with gradual changes of pore size from 50 Å ( $\gamma$ -Al<sub>2</sub>O<sub>3</sub> support layer) to 10-30 Å (surfactant-templated silica intermediate layer, depending on which surfactant was used), and then to 3-4 Å (30 nm thick microporous silica top-layer). This novel membrane synthesis and processing scheme could be potentially adapted to processing a thin, highly selective sol-gel coating on a high-surface-area polymeric hollow fiber (or ceramic monolith) support.

With the combination of high flux and high selectivity (CO<sub>2</sub> permeance of  $\sim 3 (0.5) \times 10^{-4}$  cm<sup>3</sup>(STP)/cm<sup>2</sup>-s-cmHg and CO<sub>2</sub>/CH<sub>4</sub> separation factor of  $\sim 200 (600)$ ), the dual-layer silica membrane was superior to all other reported membranes for separation of a 50/50 (v/v) CO<sub>2</sub>/CH<sub>4</sub> gas mixture. Upon further calcination, the efficiency of separating H<sub>2</sub> from constituent gases was enhanced due to shrinkage of larger pores. The membrane selectively separated hydrogen from a simulated reformat mixture (33.98% N<sub>2</sub>, 15.00% CO<sub>2</sub>, 0.997% CO, balance H<sub>2</sub>) as evidenced by the high concentration of hydrogen recovered in the permeate side stream (92 mole% H<sub>2</sub>). The CO concentration (CO is a fuel cell poison) in the permeate was reduced to at least fifty times lower than that in the feed. Beside H<sub>2</sub> purification, the membrane can also be applied to NO<sub>x</sub> removal from flue gas. NO/N<sub>2</sub> selectivity and NO permeance reached 9.3 and  $3 \times 10^{-5}$  cm<sup>3</sup>(STP)/cm<sup>2</sup>-s-cmHg, respectively. The combined strategies are proved to be effective for achieving molecular sieving in inorganic silica membranes.

The membrane formation has been proved to be highly reproducible if deposited under clean room conditions. Poor reproducibility has been found for deposition in unfiltered air (carried out in a dry nitrogen box with a humidity of 3-6 %) due to dust contamination resulting in defects in the very thin (200 nm) membranes. As shown earlier, the humidity difference between the dry nitrogen box and the clean room box (with ambient humidity) does not affect the structure of the deposited membranes.

Attempts to improve the permeance by keeping the same high selectivity were made by using the same deposition procedure under clean room condition, but employing larger pore size support tubes. Very good results were achieved with 50 Å ceramic support, promising results were achieved with the 200 Å ceramic tubes, but no good coverage was observed with the 2000 Å ceramic support. CTAB and Brij-56 seem to better cover over the rough surface of the ceramic supports, for both the 50 Å and the 200 Å supports, indicated by a lower permeance of the uncalcined surfactant-templated silica sub-layer. More recent experimental work implies that aerosol deposition is a more promising technique for directly forming mesoporous silica sub-layers on top of large pore supports (e.g. 0.2 μm α-Al<sub>2</sub>O<sub>3</sub>), as compared to conventional dip-coating which works well only with support pores of 50-200 Å.

The present dual-layer silica membrane could find large-scale use in applications such as purification of sub-quality natural gas, removal of NO<sub>x</sub> from power-plant flue gas, reduction of green house gases (e.g. CO<sub>2</sub>) and hydrogen recovery from processing gases or hydrogen purification for fuel-cell applications.

# 8

## REFERENCES

---

- [1] EPRI Report TR 106735, Inorganic Polymer Derived Ceramic Membranes.
- [2] C.J. Brinker and G.W. Scherrer: *"Sol-Gel Science"*, Academic Press, San Diego 1990.
- [3] C.J. Brinker, R. Sehgal, S.L. Hietala, R. Deshpande, D.M. Smith, D. Loy and C.S. Ashley: *"Sol-gel strategies for controlled porosity inorganic materials"*, J. Membr. Sci. 94 (1994) 85.
- [4] B.B. Mandelbrot: *"The fractal geometry of Nature"*, Freeman, San Francisco, 1982.
- [5] R. Sehgal and C.J. Brinker: *"Supported Inorganic Membranes"*, US Patent 5,772,735.
- [6] Sujit Naik: *"Zeolite-like' Silica Membranes for Isomer Separations"*, Masters Thesis, University of New Mexico, 1999
- [7] C.T Kresge, M.E. Leonowicz, W.J. Roth, J.C. Vartuli and J.S. Beck: *"Ordered mesoporous molecular sieves synthesized by a liquid crystal template mechanism"*, Nature 359 (1992) 710.
- [8] J.S. Beck et al.: *"A new family of mesoporous molecular sieves prepared with liquid crystal templates"*, J. Am. Chem. Soc. 114 (1992) 10834.
- [9] M. Ogawa: J. Am. Chem. Soc. 116 (1994) 7941.
- [10] P.J. Bruinsma, A.Y. Kim, J. Liu and S. Baskaran: Chem. Mater. 9 (1997) 2507.
- [11] M. Ogawa: *"A simple sol-gel route for the preparation of silica-surfactant mesostructured materials"*, Chem. Commun. (1996) 1149.
- [12] N.K. Raman, M.T. Anderson and C.J. Brinker: *"Template-based approaches to the preparation of amorphous, nanoporous silicas"*, Chem. Mater. 8 (1996) 1682.
- [13] Y. Lu, R. Ganguli, C.A. Drewien, M.T. Anderson, C.J. Brinker, W. Gong, Y. Guo, H. Soyez, B. Dunn, M.H. Huang and J.I. Zink: *"Continuous formation of supported cubic and hexagonal mesoporous films by sol-gel dip-coating"*, Nature 389 (1997) 364.

---

References

- [14] A. Sellinger, P.A. Weiss, A. Nguyen, Y. Lu, R.A. Assink, W. Gong and C.J. Brinker: "*Continuous self-assembly of organic-inorganic nanocomposite coatings that mimic nacre*", *Nature* 394 (1998) 256.
- [15] C.J. Brinker, Y. Lu, A. Sellinger and H. Fan: "*Evaporation-induced self-assembly: nanostructures made easy*", *Adv. Mater.* 11 (1999) 579.
- [16] D.W. Breck: "*Zeolite molecular sieves: structure, chemistry and use*", Wiley, New York, 1984.
- [17] C.J. Brinker, K.D. Keefer, D.W. Schaefer and C.S. Ashley: "*Sol-gel transition in simple silicates*", *J. Non-Crystalline Solids* 48 (1982) 47
- [18] G.C. Frye, A.J. Ricco, S.J. Martin and C.J. Brinker: "*Characterization of the surface area and porosity of sol-gel films using SAW devices*", *Mater. Res. Soc. Symp. Proc.* 121 (1988) 349.
- [19] G.C. Frye, C.J. Brinker, A.J. Ricco, S.J. Martin, J. Hilliard and D.H. Doughty: "*Sol-gel coatings on acoustic wave devices: thin film characterization and chemical sensor development*", *Mater. Res. Soc. Symp. Proc.* 180 (1990) 583.
- [20] S.L. Hietala, D.M. Smith, V.M. Hietala, G.C. Frye and S.J. Martin: "*Pore structure characterization of thin films using a surface acoustic wave/volumetric adsorption technique*", *Langmuir* 9 (1993) 249.
- [21] M.D. Thouless: "*Decohesion of films with axisymmetric geometries*", *Acta Metall.* 36(12), (1988) 3131.
- [22] K. Kusakabe, T. Kuroda, A. Murata and S. Morooka: "*Formation of a Y-Type Zeolite Membrane on a Porous Alpha-Alumina Tube for Gas Separation*", *Ind. Eng. Chem. Res.* **36**(3) (1997) 649.
- [23] R.M. De Vos and H. Verweij: "*Improved Performance of Silica Membranes for Gas Separation*", *J. Membr. Sci.* **143**(1-2) (1998) 37.
- [24] S. Naik: "*'Zeolite-like' silica membranes for isomer separation*", Masters Thesis, University of New Mexico (1999).
- [25] L.M. Robeson: "*Correlation of separation factor versus permeability for polymeric membranes*", *J. Membr. Sci.* **62** (1991) 165.
- [26] R. Quinn: "*A repair technique for acid gas selective polyelectrolyte membranes*", *J. Membr. Sci.* **139**(1), (1998) 97.

- [27] L.S. White, T.A. Blinka, H.A. Kloczewski and I.F. Wang: "*Properties of a polyimide gas separation membrane in natural-gas streams*", J. Memb. Sci. **103**(1-2), (1995) 73.
- [28] K. Kusakabe, T. Kuroda, A. Murata and S. Morooka: "*Formation of a Y-type zeolite membrane on a porous alpha-alumina tube for gas separation*", Ind. Eng. Chem. Res. **36**(3), (1997) 649.



# 9

## PUBLICATIONS AND PATENTS

---

### Publications

1. S. Prabakar, R.A. Assink, N.K. Raman, S.A. Myers and C.J. Brinker: "*Identification of self- and cross-condensation products in organically modified silica sols by  $^{29}\text{Si}$  and  $^{17}\text{O}$  NMR spectroscopy*", *J. Non-Cryst. Solids* **202** (1996) 53-60.
2. G.Z. Cao, Y.F. Lu, L. Delattre, C.J. Brinker and G.P. Lopez: "*Amorphous silica molecular sieving membranes by sol-gel processing*", *Adv. Mater* **8** (1006) 588-591.
3. N.K. Raman, M.T. Anderson and C.J. Brinker: "*Template-based approaches to the preparation of amorphous nanoporous silicas*", *Chem. Mater.* **8** (1996) 1682-1701.
4. J.P. Collins, R.W. Schwartz, R. Sehgal, T.L. Ward, C.J. Brinker, G.P. Hagen and C.A. Udovich: "*Catalytic dehydrogenation of propane in hydrogen permselective membrane reactors*", *Industrial & Eng'g. Chem. Res.* **35** (1996) 4398-4405.
5. C.J. Brinker: "*Porous inorganic materials*", *Current Opinion in Sol. St. & Mat. Sci.* **1** (1996) 798-805.
6. Y.F. Lu, L. Han, C.J. Brinker, T.M. Niemczyk and G.P. Lopez: "*Chemical sensors based on hydrophobic porous sol-gel films and ATR-FTIR spectroscopy*", *Sensors & Actuators B-Chem.* **36** (1996) 517-521.
7. Y. Lu, G.Z. Cao, R.P. Kale, L. Delattre, C.J. Brinker, G.P. Lopez (eds.: B.K. Coltrain, C. Sanchez, D.W. Schaefer and G.L. Wilkes): "*Controlling the porosity of microporous silica by sol-gel processing using an organic template approach*", *Better Ceramics Through Chemistry VII: Organic/Inorganic Hybrid Materials*, San Francisco, CA, *Mat. Res. Soc.* **435** (1996) 271-275.
8. N.K. Raman, S. Wallace, C.J. Brinker (eds.: B.K. Coltrain, C. Sanchez, D.W. Schaefer and G.L. Wilkes): "*Shrinkage and microstructural development during drying of organically modified silica xerogels*", *Better Ceramics Through Chemistry VII: Organic/Inorganic hybrid materials*, San Francisco, CA, *Mat. Res. Soc.* **435** (1996) 357-362.

9. J. Samuel, A.J. Hurd, F. van Swol, L.J. Douglas Frink, C.J. Brinker and S.C. Contakes (eds.: R.F. Lobo, J.S. Beck, S.L. Suib, D.R. Corbin, M.E. Davis, L.E. Iton and S.I. Zones): "*Preparation of microporous films with sub-nanometer pores and their characterization using stress and FTIR measurements*", *Microporous and Macroporous Materials*, San Francisco, CA, *Mat. Res. Soc.* **431** (1996) 185-190.
10. G.Z. Cao and C.J. Brinker (eds.: R.F. Lobo, J.S. Beck, S.L. Suib, D.R. Corbin, M.E. Davis, L.E. Iton and S.I. Zones): "*Gas permeation and microstructure of silica membranes prepared using an organic template approach by sol-gel processing*", *Microporous and Macroporous Materials*, San Francisco, CA, *Mat. Res. Soc.* **431** (1996) 343-348.
11. R.A. Cairncross, K.S. Chen, P.R. Schunk, C.J. Brinker and A.J. Hurd: "*Recent advances in theoretical modeling of deposition, drying, and shrinkage in sol-gel coating processes*", *Ceram. Trans.* **69** (1997) 152-158.
12. R.A. Cairncross, P.R. Schunk, K.S. Chen, S. Prakash, J. Samuel, A.J. Hurd and C.J. Brinker: "*Pore evolution and solvent transport during drying of gelled sol-gel coatings: Predicting springback*", *Drying Technology* **15** (1997) 1815-1825.
13. J. Samuel, A.J. Hurd, C.J. Brinker, L.J. Douglas Frink and F. van Swol: "*Capillary stress in microporous thin films*", *Mat. Res. Soc. Symp. Proc.* **436** (1997) 373-378.
14. Y.F. Lu, R. Ganguli, C.A. Drewien, M.T. Anderson, C.J. Brinker, W.L. Gong, Y.X. Guo, H. Soyez, B. Dunn, M.H. Huang and J.I. Zink: "*Continuous formation of supported cubic and hexagonal mesoporous films by sol-gel dip coating*", *Nature* **389** (1997) 364-368.
15. G.C. Frye, R.J. Kottenstette, E.J. Heller, C.J. Brinker, S.A. Casalnuovo, A. Sellinger, N.K. Raman, Y. Lu: "*Optimizing surface acoustic wave sensors for trace chemical detection*", *Transducers 97, Int. Conf. Solid-State Sensors: Actuators* **2** (1997) 1323-1326.
16. C.J. Brinker: "*Oriented inorganic films*", *Current Opinion in Colloid & Interface Sci.* **3** (1998) 166-173.
17. Y. Lu, G. Cao, R.P. Kale, S. Prabakar, G.P. Lopez and C.J. Brinker: "*Microporous silica prepared by organic templating: Relationship between the molecular template and pore structure*", *Chem. Materials* **11** (1998) 1223-1226.
18. C.-Y. Tsai and C.J. Brinker: "*Silica gas separation membranes prepared with surfactant-templated sublayers*", *Proceedings of the Fifth International Conference on Inorganic Membranes*, Nagoya, Japan, June 22-26, 1998.
19. C.J. Brinker, Y. Lu, A. Sellinger and H. Fan: "*Evaporation-induced self-assembly: Nanostructures made easy*", *Adv. Mater.* **11** (1999) 579-585

20. C.-Y. Tsai, S.-Y. Tam, Y. Lu and C.J. Brinker: “*Dual-layer asymmetric microporous silica membranes*”, *J. Membrane Science* **169** (2000) 255-268.
21. C. A. Click, R. A. Assink, C. J. Brinker, and S. J. Naik: “*An Investigation of Molecular Templating in Amorphous Silicas by Cross-Polarization NMR Spectroscopy*”, *The Journal of Physical Chemistry B*, **104(2)**, (2000) 233-236.

### Patents

1. N.K. Raman and C.J. Brinker: "Organic Template Approach to Molecular Sieving Silica Membranes", U.S. Patent # 5,770,275.
2. R. Sehgal and C.J. Brinker: "Supported Inorganic Membranes", U.S. Patent # 5,772,735.
3. C.J. Brinker, M.T. Anderson, R. Ganguli and Y. Lu: "Ordered Mesoporous Thin Films", U.S. Patent # 5,858,457.
4. N.K. Raman and C.J. Brinker: “Molecular sieving silica membrane fabrication process”, U.S. Patent No. 5,935,646.
5. C.-Y. Tsai, Y. Lu and C.J. Brinker: “Silica Gas Separation Membranes Prepared with Surfactant-templated Sublayers”, Filed: 6/25/1999.

